Maria Francisca Pires da Silva Carvalhão Tavares

Bachelor in Micro and Nanotechnologies Engineering

Design and Characterization of Paper-based Plasma Generators for Sterilization

Dissertation to obtain the degree of

Master of Science in Micro and Nanotechnologies Engineering

Adviser:	Dr. Diana Gaspar, Researcher, Alma Science
Co-adviser:	Prof. Dr. Luís Pereira, Associate Professor, DCM, FCT - UNL

Examination Committee:

Chairpersont:	Prof. Dr. Rodrigo Ferrão de Paiva Martins, Full Professor, DCM, FCT-UNL
Raporteur:	Prof. Dr. Hugo Manuel Brito Águas, Associate Professor, DCM, FCT-UNL
Member:	Dr. Diana Gaspar, Researcher, Alma Science

Dezembro de 2020

FACULDADE DE CIÊNCIAS E TECNOLOGIA
UNIVERSIDADE NOVA DE LISBOA

Design and Characterization of Paper-based Plasma Generators for Sterilization

Acknowledgements

Firstly, I would like to thank Professor Elvira Fortunato and Professor Rodrigo Martins, for the creation of the Micro and Nanotechonology course that I am about to graduate from and for their valuable work and dedication that made possible the development of the Centre of Investigation in Materials (CENIMAT) giving us students a wide range of opportunities to make great science.

Secondly, I would like to give a special acknowledgement to my supervisor professor Diana Gaspar. A HUGE thank you for all the support you have given me. During these times and after everything that has happened, without you my thesis would not have been possible. You are one of the kindest and hardworking people I know. Thank you for always being available, for allowing me to error and become a better researcher every day. It was a pleasure working with you. I truly am thankful, and I want to make you proud.

I would like to thank professor Luís Pereira for making it possible to work in such an innovate project that I enjoyed very much doing. Also, to Professor Aaron Mazzeo, who introduced me to this thesis and whom I had the pleasure to meet.

Moreover, I would like to thank the people in CENIMAT and CEMOP for all the help they have given me. Sara Silvestre, without you I wouldn't have had the engraved generators.

Thanks to this course I met two of the most wonderful people I know and that I get to call them my best friends. Inês and Tânia, without you, this journey would not have been the same. Thank you for putting up with me in those days when I was less bearable and listening to all my drama and dilemas. Thank you for all the good times, for all the parties, for all the craziness and specially thank you for supporting me always. Thanks to my Nô for always being there for me, I am so grateful for our friendship. Thanks to my Inês Branco for all the talks and coffees we had, you were definitely one of the most pleasant surprises of these years. Thanks to Diogo and Tomás for being the best guy friends I have ever had. To Micas, Edu, Pedro e Tomás for continuing to allow me to be part of their lives. To Narciso, Xavier, and Centeno for showing me what having fun and enjoying the moment is all about. Also, a big thank you to all the amazing people I have met during these five years of college, you made this course a lot easier. Finally, a special thank you to my cunhadinha, our friendship means a lot.

Bia, Mary, Anocas and Paula you are my second family, my sisters, my forever bestfriends. I couldn't have done it without your support and friendship. Thank you for making every moment I spend with you the best I have ever had. I will carry you for life.

Lastly, but without a doubt the most important and special thank you goes to my family. I am what I am today thanks to them. Thank you to my parents, for providing me an exceptional education, for making all of this happen, for always being there for me, and for being the best parents anyone could ever ask for. You are an inspiration. To my brother and my sisters, you are my everything. To avô Tó e avó Clarinha, I hope one day to be half the person they are. A big thank you to tia Cau, tia Guida, tio Pedro and tio Pinto, I wished everyone could have aunt and uncles as good as you are. To my cousins, António, Ricardo, Maria e Margarida. My second brothers and sisters, life would be very boring without you. Then to my grandmother avó Céu, to Didi, to Tatão, and to my cousins Alfredo and Beatriz, whom I care a lot.

Thank you to my amazing family, this work is dedicated to you.

Abstract

Nowadays, proper sterilization of surfaces, objects, and even ourselves is a constant need. This work describes the fabrication and thorough characterization of simplistic and disposable plasma-based generators for microbial disinfection, made from metalized paper with aluminum in reference to a previous design developed by Mazzeo *et al*. These devices rely on the working principle of the dielectric barrier discharge and the generation of plasma was carried out inside a vacuum chamber where different atmospheres were tested. The experimental results demonstrated that additional layers of materials with higher resistance to corrosion and oxidation than aluminum brought no improvements or advantages to reduce the surface degradation by plasmas. These paper-based plasma generators' optical emission spectra indicated that many reactive species desirable in applications such as biological decontamination are produced in the glow discharge. On another note, these generators achieved tolerable biological temperatures ($T<40$ ºC), representing an excellent approach to the generation of non-thermal plasmas ($T<70$ ºC). Beyond their characterization, this thesis demonstrated these devices' ability to generate plasma on a reduced scale and a possible optimization method of the decontamination process through plasma confinement. Towards these paper-based generators' stability, they were capable of generating plasma that lasted for more than one hour.

Keywords: plasma, dielectric barrier discharge, paper-based plasma generators, sterilization, miniaturization

Resumo

Hoje em dia, a esterilização adequada de superfícies, objetos, e mesmo de nós próprios é uma necessidade constante. Este trabalho descreve o fabrico e caracterização minuciosa de geradores de plasma simplistas e descartáveis, para a desinfeção microbiana, feitos de papel metalizado com alumínio em referência a um design previamente desenvolvido por Mazzeo *et al.* Estes dispositivos baseiam-se no princípio de funcionamento da descarga da barreira dielétrica e a geração de plasma foi realizada dentro de uma câmara de vácuo, onde foram testadas diferentes atmosferas. Os resultados experimentais demonstraram que as camadas adicionais de materiais com maior resistência à corrosão e oxidação do que o alumínio não trouxeram melhorias ou vantagens na redução da degradação da superfície pelo plasma. Os espectros de emissão ótica destes geradores indicaram que muitas das espécies reativas desejáveis em aplicações tais como a descontaminação biológica são produzidas na descarga luminescente. Por outro lado, estes geradores alcançaram temperaturas biológicas toleráveis (T<40 ºC), representando uma excelente abordagem à geração de plasmas não térmicos (T<70 ºC). Para além da caracterização destes geradores, esta tese demonstrou a capacidade destes dispositivos de gerar plasma a uma escala reduzida e um possível método de otimização do processo de descontaminação através do confinamento do plasma. Relativamente à estabilidade destes geradores de plasma em papel, estes foram capazes de gerar plasma com uma durabilidade superior a uma hora.

Palavras-chave: plasma, descarga de barreira dielétrica, geradores de plasma em papel, esterilização, miniaturização

Contents

List of Tables

List of Figures

Acronyms

a.c. – alternate current

ATR – Attenuated Total Reflectance

ATR-FTIR – Fourier-transform infrared spectroscopy with attenuated total reflectance

CEMOP – Centre of Excellence in Microelectronics Optoelectronics and Processes

CENIMAT – Centro de Investigação de Materiais

DBD – dielectric barrier discharge

d.c. – direct current

DSC – differential scanning calorimetry

EIS – electrochemical impedance spectroscopy

EDX – energy dispersive X-ray spectroscopy

FTIR – Fourier-transform infrared spectroscopy

GAl – generator with the top electrode of aluminum

GAu – generator with the top electrode of gold

GTi – generator with the top electrode of titanium

LDPE – low-density polyethylene

LPC – liquid packaging cardboard

NIST – National Institute of Standards and Technology

OES – optical emission spectroscopy

PECVD – plasma enhanced chemical vapour deposition

rf – radiofrequency

ROS – reactive oxygen species

RONS – reactive oxygen and nitrogen species

RNS – reactive nitrogen species

RGB – red, green, blue

sccm – standard cubic centimeters per minute

SEM – scanning electron microscopy

STA – simultaneous thermal analysis

TGA – thermogravimetric analysis

ULS – universal laser system

UV – ultra-violet

XRD – x-ray diffraction

List of Symbols

C – capacitance per unit area

f – frequency

P - porosity

Z – impedance

θ - Bragg angle

2θ - Angulas position

$\rho_{cellulose}$ – cellulose density

ρ_{sample} – apparent density of a cellulosic sample

Motivation and Objectives

Ever since the appearance of a new highly infectious respiratory disease, maintaining proper sterilization of surfaces, objects, and even ourselves has become imperative now more than ever. In recent years, plasma-based treatments have gained increasing attention for their potential usage in the inactivation of pathogenic microorganisms. Nevertheless, conventional plasma decontamination is limited by their inflexibility in accessing difficult areas where microbes might collect. Such a challenge appears not to be the case for paper-based technologies. Due to paper's porosity, gases' permeability is achieved, providing fuel for the plasma while cooling it down. Hence, these properties make paper a promising material for plasma generators, with a vast potential to reduce healthcare-associated infection in varied urban and rural environments. A study made by Mazzeo *et al.* reports disposable paper-based atmospheric plasma generators using the working principle of the dielectric barrier discharge, which proved to be very efficient in the inactivation of *Escherichia coli* and *Saccharomyces cerevisiae* [1]. Despite their significant progress on this matter, more investigation needs to be done to develop safer and better-optimized plasma devices for human usage. Therefore, this thesis's primary focus is to extensively study and characterize this type of generator's design to optimize and improve its performance during plasma generation. In this manner, the influence of using different electrode types and discharge gases on surface degradation by plasma will be assessed. A key objective is to understand the dependency of plasma generation effectiveness on input power and pressure. Furthermore, one of the principal goals of this research is to investigate the reactive species present in the generated plasma, considering that growing evidence has shown that the microorganisms' inactivation is due to the reactive species produced in the plasmas.

Nonetheless, these devices' ability to generate plasma on a miniaturized scale is of great interest and was tested. The reduced dimensions enable low-power sources with small footprints suited for integration in microsystems, portable devices and applications where reduced plasma generators are needed, such as the medical sector. Finally, plasma confinement in these generators was attempted using a commercial magnet in their structure.

1 Introduction

By the end of 2019, the whole world was shaken with the news of a novel, highly infectious respiratory disease, which was later declared, by the World Health Organization, as a global pandemic. Illnesses that cause pandemics are most often viral and highly contagious. Therefore, it is crucial to maintain proper sterilization of surfaces, objects, and even ourselves. The inactivation of microorganisms is generally of great interest, not only for viral infections but also plays a significant role in the food industry and medical sector in particular in the decontamination of pharmaceutical and medical devices [2], [3].

1.1 Sterilization

Sterilization is the killing or removal of microorganisms (such as bacteria, viruses, and fungi) on a surface, object, or specific region to prevent infections. Different methods of sterilization have been used in both the medical and food industry. For instance, steam and dry heat sterilization, chemical-based sterilization, and gamma irradiation are some of the standard techniques to sterilize instruments and materials and have been employed mostly in hospitals and medical divisions [4], [5]. However, these conventional techniques have certain drawbacks that can prevent the sterile material from maintaining its properties, often operate with large and bulky devices, are expensive to manufacture, use significant resources (select chemicals and chambers) and processing times [4]. In recent years, due to the demand for healthier lifestyles with fresh or minimally processed food, microbial safety needs to be guaranteed. Traditional sterilization is achieved by applying high-intensity heat to food products. Nevertheless, these methods often lead to changes in the nutritional value and losses of sensory qualities, such as flavor or texture, of the final products [3], [6].

Overall, each current sterilization technique has its limitation. As a result, recent works have been focused on developing new sterilization technologies. An optimal sterilization process needs to be effective, cost-efficient, have low processing times, non-toxic, environmentally friendly, energy-efficient, and does not stress the sterilized device [7]. For instance, a breakthrough in this area was the correlation between non-thermal plasmas and their application in the inactivation of microorganisms, which will have the potential to alleviate the disadvantages and shortcomings of the sterilization methods currently in use [8].

1.2 Plasma and its classification

As it is commonly spoken, the matter can appear in three states: solid, liquid, and gaseous. Over the years, the properties of matter in a fourth state, also referred to as plasma, have received increased attention. William Crookes firstly discovered plasma in 1897, but it was not until 1929 that this fourth state was introduced into physics by Irving Langmuir and Tonks. Plasma is an excited ionized gas that contains different concentrations of low-molecular reactive atoms, ions, molecules, radicals, and emits numerous kinds of electromagnetic radiation such as infrared, visible, and ultraviolet (UV) [9].

Plasmas can be categorized as thermal or nonthermal based on the relative temperatures of their electrons, ions, and neutrals [10]. In thermal plasma or equilibrium plasma, the electron and gas discharge temperatures are high and achieve an energetic equilibrium, resulting in high gas temperatures [11]. On the other hand, in nonthermal or non-equilibrium plasma, the processes are driven by electrons, while the majority of gas atoms, ions, and molecules remain in a low-energetic state leading to a low-temperature plasma. This unique characteristic instigated the possibility of using nonthermal plasmas for the treatment of temperature-sensitive materials and biological matter [12], [13]. Nonthermal plasmas can operate under moderate temperatures (below 70 ºC), thus, thermal and chemical damage to the substrate is limited. Besides, the antimicrobial efficiency of these plasmas is incontestable and can provide sterilization within a few seconds[1], [14], [15].

1.3 Generation of Nonthermal Plasmas

Plasma can be generated by various methods, including gas discharge, photoionization, heat radiation, radio frequencies, to name just a few. Among these methods, gas discharge is the most common way to generate nonthermal plasma [3].

The application of nonthermal plasmas firstly started with experiments on microorganism inactivation using low gas pressures. Researchers showed that an electrical discharge at low pressure using an appropriate gas (for example, oxygen or its mixture with nitrogen - N_2/O_2) resulted in sterilization. However, even though the use of vacuum plasmas was a significant improvement to the existing sterilization methods, it still has some limitations, particularly the need for batch processing, long processing times, and high costs [16].

For this reason, more studies have been done in developing atmospheric-pressure plasma devices for sterilization purposes, also known as cold atmospheric plasma devices. Because of the open atmospheric conditions, excited and ionized atoms or molecules interact with other atoms or molecules of the working gas and neighboring media, leading to the generation of reactive species with biological potential. Consequently, a wider variety of active plasma species are involved in the sterilization process (Hydroxyl radical (OH), Hydrogen Peroxide (H2O2), Peroxynitrite (ONOO-), Nitric Oxide (NO), and Argon metastable) [12].

Atmospheric pressure cold plasma devices can operate below 40 ºC or be applied in a pulsed mode, which prevents an overheating of the object, surface, or tissue where it is being applied. Depending on the plasmas source, setting, and proximity of the discharge to the substrate, pathogens can be eliminated either by direct contact or by remote treatment mode [17]. In the former, the plasma is in direct contact with the target area, while in the latter, the plasma generated containing the reactive species is transported onto the substrate via a carrier gas or by diffusion. Atmospheric-pressure discharge for inactivating pathogenic microorganisms is generated in a variety of ways: dielectric barrier discharge (DBD), plasma jet, and corona discharge are the most commonly used sources for cold plasma.

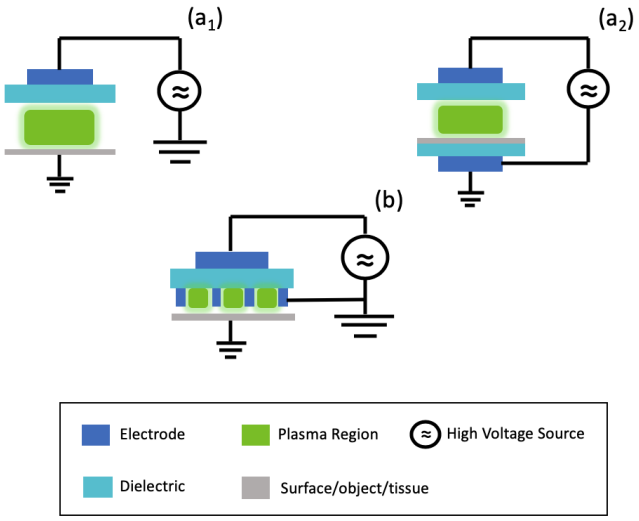

Figure 1.1 - Basic configurations of DBDs: (a) volume DBD (1- Single layer, 2- Double layer); (b) surface DBD.

In the late '90s, the first experiments were conducted by Larrousi on the inactivation of bacteria using one of the most used cold plasma sources, the DBD reactor [18]. This device consists of one or two electrodes, with at least one of them covered with a dielectric layer to prevent spark formation by limiting the discharge current and restricting the gas's heating. Usually, plasma is generated by applying high sinusoidal voltages to one of the electrodes, resulting in a sufficiently

high electric field suitable to produce ionization of the gas in/above the gap between the electrodes [18]. During this process, free electrons, accelerated by the electric field, ionize the gas, and electronic avalanche is generated, followed by the propagation of a thin, weakly ionized plasma channel called a streamer. The electrical breakdown of the gas leads to the charging of the dielectric's surface; as a result, the accumulation of charged particles on its surface induces an electric field opposed to the applied one, and thus, the total electric field is decreased, and the discharge extinct in a few tens of seconds. After the polarity reverses, the deposited negative charges facilitate new avalanches and streamers in the same location.

The distance of the electrodes is from micrometers up to centimeters according to the used process gas and operating voltage. Moreover, depending on the device's setup, two types of plasma are generated, volume or surface plasma (**Figure 1.1**). In volume plasma, one or both electrodes are covered by a dielectric layer, or this dielectric layer separates the gas gap. Whereas in surface plasma, both electrodes are in direct contact with the dielectric layer. Alongside the dielectric barrier discharge is the resistive barrier discharge. In the latter one, the dielectric insulator is replaced by a highly resistive material, covering one or both electrodes. Apart from behaving as a resistive load, this modified version also makes it possible to operate plasma by DC high voltages [19].

When plasmas are generated within dimensions ranging from few micrometers up to a few millimeters, they are designated as microplasmas or micro discharges. Due to their reduced dimensions, they represent an economic and ecological alternative for conventional technologies and are well suited for integration in microsystems and portable devices. Microplasmas are a promising concept in this area and an emerging field of nonthermal plasma devices. Indeed, owing to their ability for microbial decontamination, they are receiving growing attention in biomedical, food, and environmental industries [20].

1.4 Emerging role of Paper-based Technologies

In the present time, plasma-based generators frequently use rigid constituents, which cannot bend or conform to irregularly shaped objects. As a result, the lack of flexibility limits their potential use in accessing narrow areas where microbes might collect. Therefore, the need for scalable and easy to manipulate atmospheric plasma generators arises.

Over the years, paper-based technologies have been increasingly attractive within the scientific community; they are affordable, environmentally friendly, foldable, and scalable for manufacturing [21]. Paper is mostly made up of cellulose fibers, and its orientations and surface morphology fulfil the requirements of various types of paper products. Regarding its application for plasma generation, the cellulose-based paper is capable of handling temperatures up to 250 ºC and is known for possessing a porous structure. Due to such properties, it seems like paper is a suitable material for atmospheric plasma generators.

In 2012, a study conducted by Cheng-Che *et al.* aimed to fabricate a plasma-generating device on a paper substrate using a screen-printing technique. Carbon paste electrodes were printed to a silkscreen coated with a photosensitive emulsion. This research demonstrated that as well as being sustained by means of dc power source in a helium atmosphere, plasmas can be kept stable when flat, rolled or folded along various orientations [22]. "Paper-based plasma sanitizers" by Aaron D. Mazzeo and his research group records a recent approach to plasma-generating devices by fabricating a disposable and straightforward plasma generator, using metalized paper capable of antimicrobial sanitization. This experimental work demonstrated that these plasma sanitizers deactivated more than 99% of *Saccharomyces cerevisiae* and 99.9% of *Escherichia coli* cells within 30 s of noncontact treatment. Besides, it shows how paper-based generators are conformable to curved surfaces, compatible with user interfaces, and suitable for the sanitization of microbes [1].

In this line of work, the present study focused on developing elementary, low-cost paper-based microplasma generators using the working principle of the DBD, based on the previous work reported by Mazzeo *et al.* The preliminary attempt to generate plasma using the fabricated devices was conducted within an adapted vacuum chamber where three different discharge gases were used: argon, air, and nitrogen. Our devices were capable of generating plasma that lasted for more than one hour and generated many reactive species desirable for biological decontamination.

1.5 Sterilization by Nonthermal plasmas

Of the many applications of this novel technology, possibly the most extensively studied and comprehensively established is the antimicrobial effect of nonthermal plasmas. As mentioned above, since the first studies in the late ’90s, atmospheric plasma generators have shown to inactive a broad range of microorganisms, such as Gram-negative and Gram-positive bacteria, biofilm-forming microorganisms, and viruses [23]. Their bactericidal effect has proven to be very effective even with the deadliest or most resistant microorganisms, for example, *Escherichia Coli*, *Staphylococcus aureus*, and *Bacillus Subtilis* [1], [24], [25].

As reported by Xinyu Liao *et al.*, the efficacy of these nonthermal plasma sources depends on several processing variables, including input power (voltage and frequency), treatment time, working gas, flow rate, and exposure mode. Different investigations have shown that the higher the frequency and input voltage, the greater the inactivation of microorganisms [26][27]. Moreover, it has been shown that the choice of working gas type determines the category and level of production of reactive species by nonthermal plasmas [28]. Indeed, Lee *et al.* demonstrated that the addition of oxygen helped to produce more radicals, thereby increasing the antimicrobial effect [29]. Notwithstanding, they also mentioned that the antimicrobial effect of nonthermal plasmas is also affected by two other factors, such as environmental elements and microbial properties. Environmental conditions like pH or humidity have a significant impact on the sterilization efficacy of this technology. For instance, increasing the relative humidity leads to a higher generation of radicals, thus positively affecting plasmas sterilization [30]. Just as important, microbial properties have a significant influence on the inactivation efficacy of nonthermal plasmas. For example, Gram-negative bacteria show more plasma sensitivity than Gram-positive bacteria; this is due to Gram-negative’s bacteria thinner outer membrane [31].

A critical challenge that remains for plasma technology it is the understanding of the mechanisms that underly microbial inactivation by nonthermal plasmas. For instance, the oxidative damage of membranes, such as membrane lipid peroxidation, and intracellular components are thought to be two possible mechanisms of killing bacteria through nonthermal plasmas. The vulnerability of the membrane lipid is thought to be due to its location near the cell surface and sensitivity to reactive oxygen species (ROS) [32]. Another factor that is believed to be responsible for microbial inactivation is ROS's ability to induce intracellular oxidative stress and programmed cell death in mammalian cells [33].

Apart from all these biological phenomena, various physical mechanisms are also responsible for the inactivation of microorganisms through nonthermal plasmas. The most studied is electrostatic disruption. Mendis *et al.* explained that the electrostatic forces generated by the charged particles, produced by plasma, on the cell surface increase and overcome tensile strength resulting in the instability of the cell wall and following death [34]. Finally, yet importantly, it is electroporation. Electroporation is the formation of pores in cell membranes leading to content leakage and cell death. In direct contact treatment, the cell walls become the second electrode enabling a sufficiently strong electric field to disrupt cell membranes [35].

1.5.1 Biomedical Applications of Nonthermal Plasmas

Due to continued research efforts on plasma science and groundbreaking investigations, considerable progress was made over the past years. The impact of microplasmas upon biology

and medicine is inevitable, and the biomedical applications of such technology are an excellent example of their tremendous potential. They include sterilization, polymer material preparation, wound healing, tissue or cellular removal, dental treatment, and cancer therapy [19], [23].

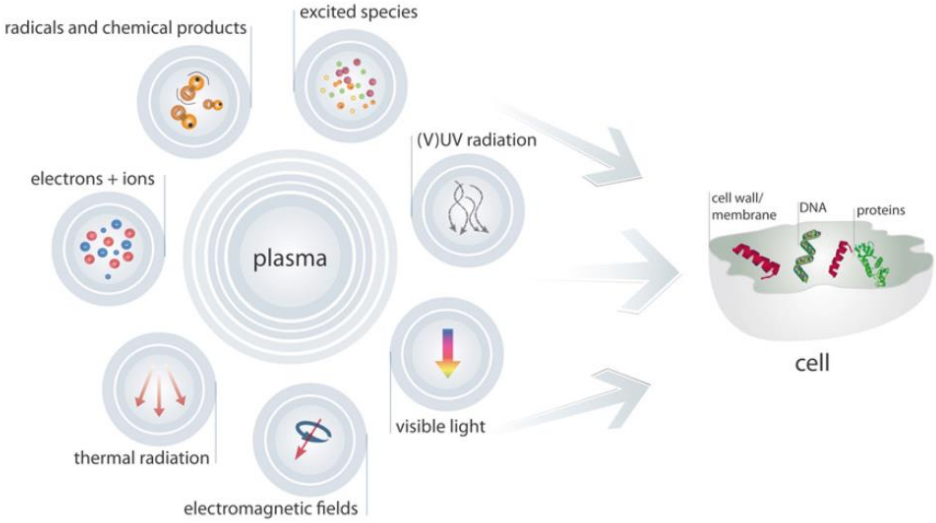

Figure 1.2 - Schematic of Plasma-cell interaction [9].

Plasmas have proven to be highly beneficial for the medical sector. This is because when generated at near-room temperature, plasma provides a rich environment of reactive plasma species and energetic charged particles (**Figure 1.2**); however, it is becoming increasingly evident that its biological effects on cells and tissues is due to the production and efficient delivery of reactive oxygen and nitrogen species, also known as RONS, similar to those naturally produced in physiological and biochemical processes in the cells. Some RONS of relevance to plasma medicine are hydroxyl radical (OH), hydrogen peroxide (H_2O_2), peroxynitrite ($ONOO^-$), and nitric oxide (NO). One significant advantage of RONS is their nontoxicity effect on the human body. Because of their occurrence in typical cell processes, mammalian cells have protective mechanisms that prevent the body from reaching to unwanted and harmful levels of these species. Thus, there is no increased risk of treatment from a localized and short-term generation of microplasmas [12].

As pointed out by K-D Weltmann and Th Von Woedtke the most significant biological implications of cold atmospheric plasma sources are the inactivation of a broad spectrum of microorganisms, even those resistant to antibiotics [12]. Depending on the plasma treatment intensity, as well as stimulating cell proliferation and tissue regeneration, they can inactivate cells by initialization of programmed cell death (apoptosis). Despite plasmas outstanding characteristics, much more work and careful investigations need to be done, especially on the understanding of the biochemical pathways and physical mechanisms whereby plasma affects cells. Nevertheless, its biomedical application seems to have a promising outlook.

2 Materials and Methods

2.1 Plasma-generating device design and fabrication

These generating-plasma devices have two essential components: the dielectric material and the electrodes. In this investigation, the substrate used to manufacture the generators was liquid packaging cardboard (LPC) and it is produced by the Finnish company *Stora Enso*. It is composed of three layers: (i) cardboard, made of pressed cellulose fibers and acts as the dielectric material (ii) an adhesive layer made of low-density polyethylene, and (iii) an aluminum (Al) sheet, that forms the powered electrode[36].

Their fabrication involved four steps: (i) design of different configurations, (ii) coating the top electrode with different metals, (iii) laser-pattern engraving, and (iv) the miniaturization of these devices. The second and fourth steps are facultative.

2.1.1 Design of Electrode Configurations

For the generation of plasma two different electrode configurations of these paper-based plasma generating devices were considered, as shown in **Figure 2.1.**

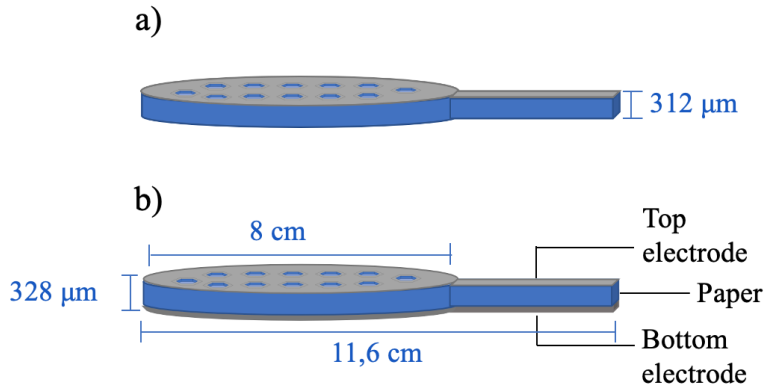

Figure 2.1 – Schematic of different configurations of plasma generators made from metallized paper: (a) First configuration; (b) Second configuration.

As illustrated in **Figure 2.1a**, the grey colored racket outlining the top electrode represents the thin Al conductive layer (6-7 µm) of the packaging cardboard, being the cellulose fiber layer, both the dielectric and grounded electrode. The honeycomb design was patterned on the top electrode with an overall diameter of 8 cm, forming the two-electrode configurations' powered electrode (**Figure 2.1**). The second configuration (**Figure 2.1b**) is based on the previous design, but with the addition of a thin conductive layer of Al (≈100 nm) deposited on the back side, forming the grounded electrode.

2.1.2 Coating with different metals

During the fabrication of these generators, it was essential to study the relevance of surface degradation of the aluminum layer and how different electrode types on its generation influence the plasma generation. For this reason, Electron-beam assisted thermal evaporation was used to deposit thin films of gold (Au) and titanium (Ti) (60 nm) on the top electrode (**Table 2.1**) and was carried out in a system designed and built at CEMOP/UNINOVA. Both depositions were made at room temperature with a base pressure around $6x10^{-6}$ mbar, and growth rate of 0.1 nm/s. An image of the differently coated samples is available in the annexes section (**Figure A 1**).

2.1.3 Laser-based Patterning

In the paper-based plasma generators, repeated hexagons (similar to honeycombs) were patterned, to form the top electrode, using a laser. Previous studies showed that such a pattern allows a uniform distribution of the operational voltage across the surface area, enabling the generation of plasma over the entirety of the patterned surface, and along the edges of the hexagonal grid. On top of that, it uses a minimal amount of total perimeter to cover a surface [1], [2], [37].

For this work, a pulsed fiber laser cutting system (Universal Laser System (ULS)) was used, with a wavelength of 1,6 μm. The honeycomb-like patterns were previously designed with image software (Adobe Illustrator CC) and imported into the computer-controlled laser system. Using a Red, Green, and Blue (RGB) color code, different settings of frequency (30 or 100 kHz), power, and speed can be obtained within the same sample. Firstly, a variation of the parameters mentioned above was employed: (i) frequency, (ii) power, and (iii) speed. After analyzing the effects produced on the differently coated samples, it was possible to optimize the best engraving conditions to obtain the desired pattern and prevent a short circuit of the device.

2.1.4 Miniaturization of the Plasma Generators

In order to investigate the generators' potential on a reduced scale, a study was carried out to evaluate both the maximum spacing resolution between two lines and the maximum resolution of a drawn line by the laser engraver. The intended honeycomb-like patterns were obtained using the optimized engraving conditions previously studied. Snapshots of the resolution analyses and a comparison of a normal generator and the miniaturized one are shown in the Annexes section (**Figure A 2** and **Figure A 3**).

2.2 Plasma generation

The experiments were conducted within an adapted vacuum chamber to generate plasma at low pressures of 0.5-8 Torr using three different atmospheres: air, argon, and nitrogen. A generator at a frequency of 13.56 MHz was used.

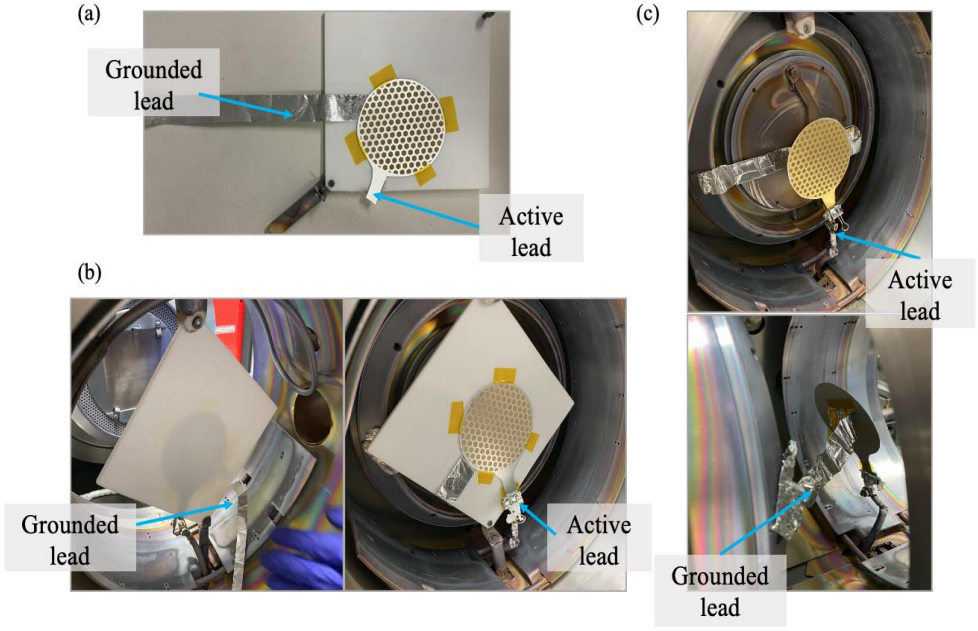

Figure 2.2 - Experimental set up for generating plasma: (a) Sample's preparation. (b) Initial arrangement of the sample inside the chamber. (c) Improved arrangement inside the chamber.

In early experiments, firstly, the generator was fixed, using Kapton tape, on a (15 cm)×(14 cm) rectangular Teflon base, where an aluminum connector was previously glued, that contact the bottom electrode, remaining grounded at all times (**Figure 2.2a**). The power is applied to the edge of the lead of the generator, as shown in **Figure 2.2**.

After performing many experiments, it was possible to develop a new type of setup, with the advantage of allowing a better view of the generators while generating plasma. In this case, the Teflon base is dismissed, and the generator is fixed using a clamp. The power is applied to the generator's end, whereas the aluminum connector is bonded directly to the bottom electrode and kept grounded (**Figure 2.2c**).

In all studies, the base pressure of the chamber was at about 0.18 Torr. The gas was introduced into the chamber with a flow rate of 20 sccm, except for the air where the flow was controlled by a needle valve. The ultimate partial pressure was at about 0.38 Torr.

2.3 Characterization Techniques

2.3.1 Structural, morphological, and compositional characterization

2.3.1.1 X-ray diffraction

X-ray diffraction (XRD) is a non-destructive technique that was used to collect information on the structure of the paper-based generators. The results were obtained using an X-ray diffractometer (PANalytical X'Pert PRO MRD) with a Cu Kα radiation source to scan the samples, which were recorded in a 2θ range from 10° to 90°.

2.3.1.2 Porosity

The porosity of the packaging cardboard was estimated according to equation 1:

$$P(\%) = \left(1 - \frac{\rho_{sample}}{\rho_{cellulose}}\right) \times 100 \qquad \text{Equation 1}$$

Where $\rho_{\text{cellulose}}$ is the density of cellulose with a tabled value of 1.5 g cm^{-3} [38], and ρ_{sample} is the apparent density of the sample (g cm^{-3}).

2.3.1.3 Scanning Electron Microscopy

Before and after generating plasma, the generators' morphological and compositional analyses were performed using a scanning electron microscope (SEM, Hitachi TM3030 Plus) equipped with an energy-dispersive X-ray spectroscopy measurement (EDX, Oxford XMax 150).

2.3.2 Optical characterization

2.3.2.1 Fourier-transform infrared spectroscopy

The chemical analyses of the generators were performed by Fourier-transform infrared spectroscopy (FTIR, Thermo Nicolet 6700 Spectrometer). The spectra were acquired between 4500 and 500 cm^{-1} using an attenuated total reflectance (ATR) sampling accessory (Smart iTR).

2.3.2.2 Optical Emission Spectroscopy

Optical Emission Spectroscopy (OES) was used to identify the reactive species present in the generated plasma. The spectrums were obtained using an optical fiber placed at a quartz viewpoint of the chamber and connected to a spectrometer (Ocean Optics HR4000). These measurements were collected using a spectral range of 200 to 1100 nm, and an integration time of 2 seconds.

2.3.3 Electrical characterization

2.3.3.1 Electrochemical Impedance Spectroscopy

The characterization of the packaging cardboard's electrical properties was conducted using Electrochemical Impedance Spectroscopy (EIS, Potentiostat 600TM Gamry Instruments), but in this case, potentiostatic impedance spectroscopy analyses were performed. For these measurements, the sample was cut in the form of circles with a diameter of 1 cm and placed between a gold and aluminum electrodes, which were connected to an earth lead, reference electrode, counter-electrode and working electrode. The potentiostat has a frequency range of 1 Hz to 1 MHz, an applied AC voltage of 5 mV rms.

2.3.4 Complementary characterization techniques

2.3.4.1 Differential Scanning Calorimetry

For this study, the Simultaneous Thermal analysis (STA) was used to determine the cellulose membranes' thermal stability. Using this analysis, data from the thermogravimetric analyses (TGA) and the differential scanning calorimetric (DSC) measurements are obtained simultaneously in the same instrument (TGA-DSC-STA 449 F3 Jupiter, Netzsch). The results were collected under an atmosphere of nitrogen, with a 30 ml/min flow rate, using a temperature range of 20 to 550 K with a 5 K/min step.

3 Results and Discussion

This chapter presents and discusses all the work done regarding the generators' fabrication and generation of plasma. First, section 3.1 presents the characterization of the dielectric material. Secondly, section 3.2 briefly shows the laser parameters' optimization results to engrave the honeycomb designs on the generators' surface. Section 3.3 describes the initial studies made on the generation of plasma. In section 3.4, the comprehensive characterization of the devices after the plasma generation was performed. Finally, sections 3.5 and 3.6 provide a closer look at the plasma generation's investigation using miniaturized generators and plasma confinement using a commercial magnet, respectively.

3.1 Dielectric Barrier Characterization

As previously described in section 2.1, the substrate used for the generators was liquid packaging cardboard, consisting of three layers: (i) pressed cellulose fibers (cardboard); (ii) an adhesive layer of low-density polyethylene (LDPE); and (iii) a sheet of aluminum. LPC is a biodegradable and antiseptic material commonly used worldwide in the food processing and beverage industry [36].

The liquid packaging cardboard characterization by TG-DSC analysis (**Figure B 1**) reveals an initial weight loss (<10 %) at temperatures close to 100 °C related to the release of adsorbed water from the cellulose fibers. The thermal degradation of LPC starts around 250 °C and proceeds up to around 350 °C. Therefore, the substrate is thermally stable up to 200 °C and likely viable up to 250 °C. The XRD analyses from the LPC (**Figure B 2**) show the presence of distinct cellulose type I, given the characteristic $(1\bar{1}0)$, (110), (002), and (004) crystallographic planes at 2θ = 14.9°, 16.3°, 22.5°,and 34.3°, respectively [39], [40]. Additionally, it is possible to identify three sharp peaks in the angular position (2θ) at 44.7°, 65.1°, and 78.2°, which can be related to the (200), (220), and (311) planes, respectively, of aluminum [41]. Some properties of the LPC are listed in **Table 3.1**.

Table 3.1 - Characteristics of the liquid packaging cardboard tested.

Thickness, µm	312
Apparent density, g cm^{-3}	0.923
Porosity, %	38.44

The potentiostatic impedance spectroscopy measurements were used to evaluate the capacitance of the packaging cardboard as a function of the frequency. Through the spectra obtained (**Figure B 3**, annex section B), it is possible to observe an increase in the capacitance as the frequency is decreased as a result of an interfacial polarization, produced by the formation of an electrical double layer at the paper/electrode's interfaces [42]. These results suggest that by using paper as a dielectric material, one can obtain high capacitances at low frequencies. The transition from resistive to capacitive behavior at low frequencies can also be observed using the phase angle vs. frequency plot. Additionally, through this plot, it is possible to distinguish two more polarization mechanisms. Starting from high frequencies, the phase angle is lower than -45°, indicating a dipole's relaxation. Whereas for intermediate frequencies, the phase angle is greater than -45°, and the LPC retains a resistive response.

Since the frequency used to generate plasma rounds the MHz, with the observed results, it might be possible to infer that the plasmas produced in this study can be based, on both, a resistive and capacitive barrier discharges. As Laroussi *et al.* demonstrated, the resistive material acts as a

resistive load inhibiting the current from reaching high values, which prevents the arcing of the discharge. Consequently, this type of plasma generation produces large volume plasmas and enables the operation of the discharge in either dc or ac modes, which is a good indicator of the suitability of these generators in atmospheric conditions [43].

3.2 Optimization of the patterning parameters

One crucial aspect of the engraving process concerns the etching of the aluminum in the metalized paper resulting in the desired pattern since it is essential to avoid any short circuit on the device. The laser parameters were optimized on the differently coated substrates by patterning square-shaped patterns as a matrix, where the laser power was kept constant in each line while each column had different speeds. This process was common to both frequencies, 30 and 100 kHz. The resultant matrices can be observed in annex B. The following step was to verify the engraved squares' electrical conductivity, using a multimeter, and evaluate the three best-etched patterns. Afterward, SEM imaging was used to observe the produced patterns and help decide the final laser power, speed, and frequency conditions (annex B). The optimized parameters are summarized in **Table 3.2**.

Table 3.2 - Optimized parameters during laser-based pattern engraving.

Metal	Frequency (kHz)	Power (W)	Speed (m/s)
Al	100	35	1.14
Au	100	40	1.08
Ti	100	40	1.08

In general, higher frequency (100 kHz) led to better etching of the electrodes due to the laser's deeper penetration in the material. In the aluminum electrode, using a laser power of 35 W and a speed 1.14 m/s led to the best-engraved design. Regarding the gold and titanium electrodes, the initial analyses determined the best laser power was 25 W and laser speed was 0.38 m/s. Nonetheless, when the first honeycomb design was engraved, the conditions mentioned above did not produce the required etching. Thus, it was necessary to increase both power and speed parameters.

3.3 Generation of Plasma

In the initial stages of this study, the generation of plasma was divided into two phases. In phase I, the main goal was to test if the two generator devices worked. Depending on the generators' operation, it would proceed to phase II. Phase II's primary objective was to investigate the influence of using different atmospheres as the discharge gas upon plasma generation, and simultaneously study the dependency of parameters such as input power and pressure on its generation.

For simplification purposes, the following acronyms will be adopted to refer to the three types of generators: GAl being the generator with the top electrode of aluminum (6-7 µm), GAu the generator with a top electrode of gold (60 nm), and GTi the generator with a top electrode of titanium (60 nm).

3.3.1 Phase I study

The preliminary attempts to generate plasma began with the simplest configuration (**Figure 2.1a)**, without the bottom electrode. It was used a function generator of frequency 13.56 MHz, an atmosphere of argon, and a pressure of 0.55 Torr. This configuration was abandoned because it resulted in a dispersed and unstable plasma (data not shown). The rest of the work along this thesis was carried out employing only the second configuration. Subsequently, using the same conditions mentioned before, the three types of generators' behavior in vacuum were assessed. In this preliminary trial, the plasma generators were operated for up to 12 minutes. During the first ten minutes, the plasma was generated at 5 W and the last 2 minutes at 10 W. The results are shown in **Figure B 8**, in the annexes section. It is clear that when the device is powered, the top electrode surface area is entirely enveloped by plasma, meaning that all three types of electrodes can generate plasma in an inert atmosphere. For this reason, it was possible to proceed to phase II. The experimental set up used is described in section 2.2.

3.3.2 Dependency on input power and pressure

The dependency of plasma generation on input power and pressure was studied using three types of samples and different discharge gases, such as air, argon, and nitrogen. **Figure 3.1** represents a schematic of the experimental setup used in the generation of plasma.

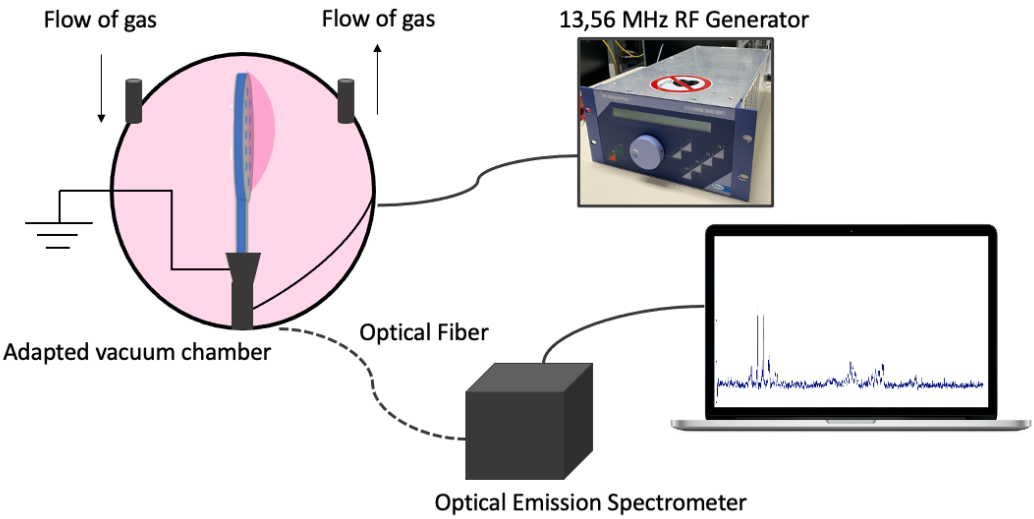

Figure 3.1 - Schematic of the experimental setup used.

Five values of power (1, 5, 10, 15, 20, and 25 W) and six values of pressure (0.55, 1, 2, 4, 6, 8, >10.5 Torr) were used. The pressure and power values were kept in each condition for 2 minutes. The increase in pressure is made by closing the exhaust valve.

3.3.2.1 Argon atmosphere

The first study to be performed used argon as the discharge gas. **Table 3.3** shows an example of the results obtained, using the generator GTi. The voltage values presented in it are intended to show the magnitude of the dc self-bias potential over the entire range of discharge conditions investigated in this study. The results for the other two types of the generator are presented in the annex B (**Table B 1** and **B 2**).

Comparing the data obtained for the three generators, the plasma was better sustained using lower pressure and higher power values in all cases. With 8 Torr, the generators began to sustain a very unstable plasma. Indeed, as shown in the annex section in **Table B 2**, for GAu, by the end of the experiment using a pressure of 4 Torr, plasma was sustained in a pulsed mode ending up in self-

extinction. The best results were achieved using the GTi, once it was possible to generate plasma at pressures higher than 10.5 Torr (also nominated as a static mode, where the exhaust valve is completely closed and there is no evacuation of the gas), as depicted in **Table 3.3**. It is worth mentioning that the three generators were capable of generating plasma that lasted for more than one hour.

Table 3.3 - Matrix of Power vs Pressure: photos obtained of generator GTi inside the chamber while generating plasma using an argon atmosphere.

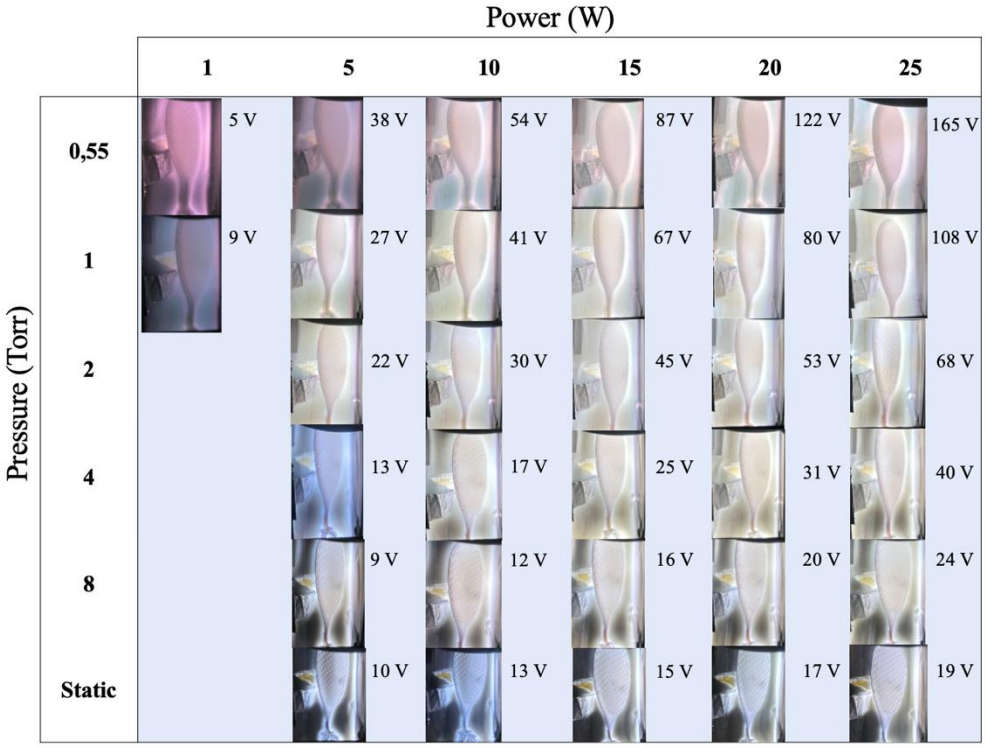

As described before, in this plasma generator, rf power is applied to the top electrode; consequently, a substantially dc negative potential, also called self-bias voltage, is generated. In other words, during a half period where the alternating current is positive, electrons in the plasma are attracted to the top electrode. In contrast, during the negative half of the applied rf power, ions in the plasma are attracted to the top electrode. Since electrons are lighter than ions, they are highly mobile; thus, the electron current collected during the first half cycle can be much greater than the current collected during the second half cycle. Therefore, during the first few rf cycles of the discharge, the electrodes collect an excess of electron current, and a negative dc bias begins to develop. Since the dc self-bias voltage enables a continuous and stable discharge and influences the ion energy present in the plasma [44], it was necessary to register the values obtained and study its behavior under different pressure and input power values and atmospheres.

For the three type of electrodes, the dc bias was found to increase as the gas pressure was reduced due to the increased mean free path of the electrons [45]. In this way, there are fewer collisions, and the electrodes collect electrons at a higher rate with higher energy. Increasing the input rf power contributed to higher dc self-bias voltage values, resulting from an increase in electron density. Moreover, the dc self-bias difference increases rapidly at lower pressures, whereas the dc self-bias difference increases slowly in the high-pressure range.

In the following experiments, the generation of plasma was performed using nitrogen and air as the discharge gases. Since one of the main goals of this study was to try to generate plasma in the high-pressure regime using lower input power values, the range of power was limited to 1, 5, 10 and 15 W.

3.3.2.2 Nitrogen atmosphere

As previously noted, plasma provides a rich environment of reactive plasma species and energetic charged particles. Nevertheless, growing evidence shows that its biological effect on the inactivation of a broad spectrum of microorganisms results from the production of reactive oxygen and nitrogen species (RONS). Hence, the need arose to test plasma generation with an atmosphere of nitrogen.

Table 3.4 - Matrix of Power vs Pressure: photos obtained of generator GAu inside the chamber while generating plasma using a nitrogen atmosphere.

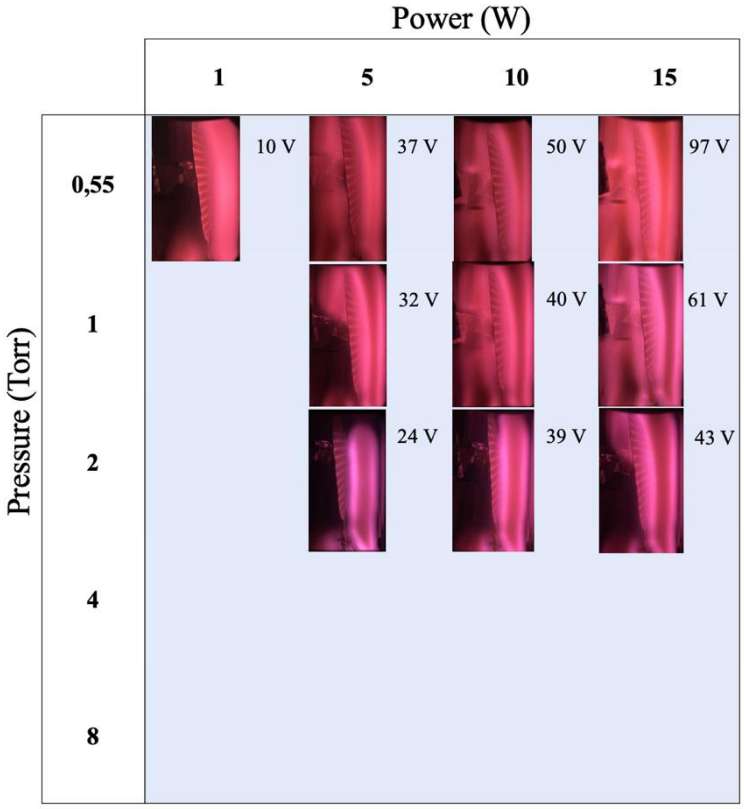

Here, the pressure is shown to reach a maximum value of 2 Torr for each generator type. For both GAl and GTi, they could ignite a discharge at 4 Torr. However, plasma was not covering the entire surface area of the generator, and these results were discarded. Regardless, GAl was the only generator able to generate plasma at a minimum input power value (1 W). **Table 3.4** represents the photos obtained of the chamber's interior for the generator GAu. The remaining data is provided in the annex section B (**Table B 3** and **B 4**). In this case, plasma lasted for almost thirty minutes, which is still a considerable plasma generation interval.

When using nitrogen as the discharge gas, the dc self-bias potential presented similar values to those observed in an argon atmosphere. Overall, the dc self-bias potential also increased with input power and decreased with the pressure applied.

3.3.2.3 Air atmosphere

The last tests were carried out, by admitting air to the chamber. This aimed to mimic an atmospheric environment since one of the future purposes of these generators' fabrication is to generate plasma at atmospheric conditions (pressure and surrounding environment).

Since atmospheric air is composed mainly of nitrogen (78.08%), the dependence on pressure and input power for the three types of devices is found to be similar to those observed in the nitrogen atmosphere. Generators GTi and GAu only sustained plasma until 2 Torr (**Table B 5** and **B 6**).

Simultaneously, generator GAl revealed to be the best type of electrode, having been the only generator to ignite a stable discharge at 4 Torr, as illustrated in **Table 3.5**.

Table 3.5 - Matrix of Power vs Pressure: photos obtained of generator GAl inside the chamber while generating plasma using air as an atmosphere.

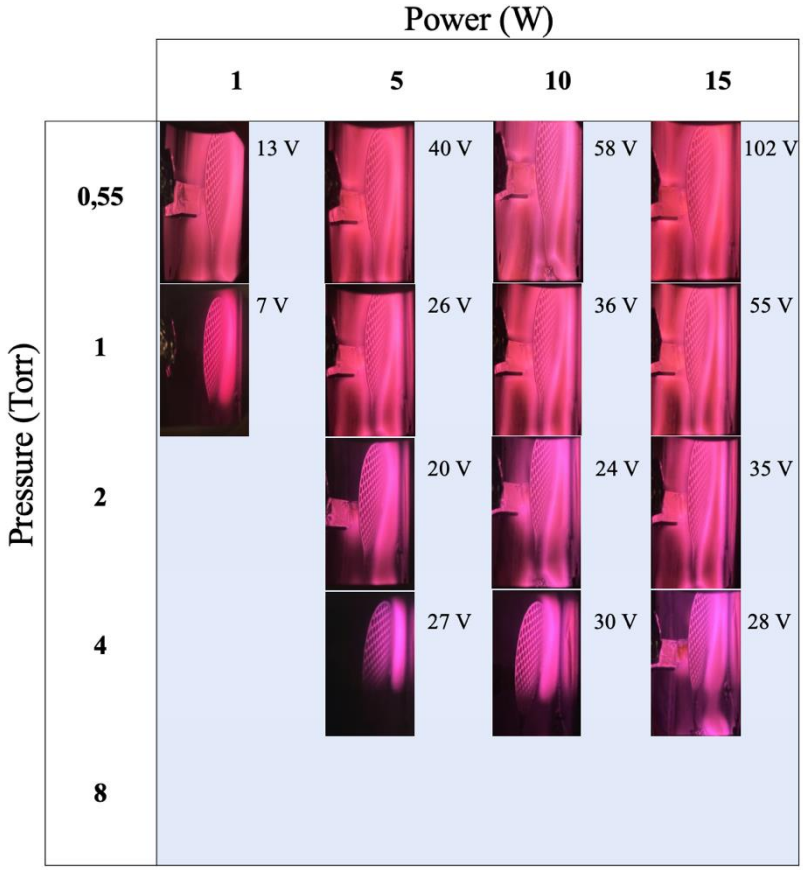

The tendency of the dc self-bias potential to increase with the increase of input rf power and decrease in pressure is also noted under this atmosphere. Moreover, as reported in the literature, the type of gas used in the process yields different results for these potentials [44]. Indeed, argon as the discharge gas resulted in the highest dc self-bias voltages. On the contrary, using air as the atmosphere resulted in the lowest values. **Table B 7**, in annex B, exemplifies the influence of different gas types in the dc self-bias potential.

3.4 Composition and morphology

3.4.1 Chemical and Morphological Analyses

To observe the effects of prolonged plasma generation throughout the device, SEM imaging was realized on both the dielectric and electrode surfaces before and after plasma generation using the different discharge gases. In every electrode type, the laser cutting system produced finger-like shaped filaments around the edges of the honeycomb design. As shown in **Figure B 9**, for all cases, after generating plasma, it is possible to observe a reduction of those filaments, indicating a mild degradation of the generators.

Generator GAl presents the least amount of degradation and surface modification effects after a long plasma generation period. There is slight curling of the aluminum layer on the honeycomb's edges in every atmosphere, and a small number of nanoparticles spread over the dielectric surface. Nonetheless, these changes are more evident when using nitrogen and air as the discharge gases

(**Figures 3.2b** and **3.2c**). These results are expected, resulting primarily from their reactive behavior when compared to argon, an inert gas.

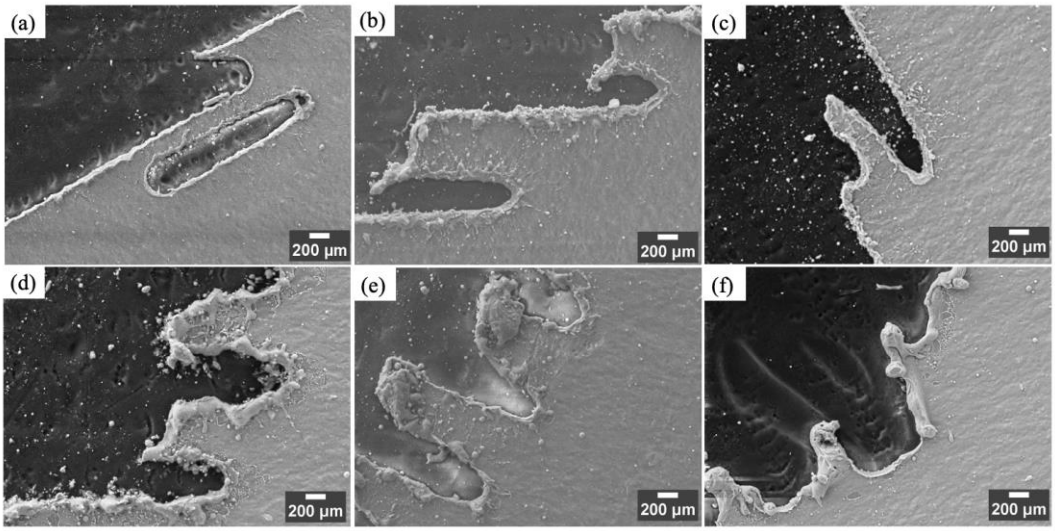

Figure 3.2 - (a-c) SEM images of generator GAl after generating plasma using argon, nitrogen, and air as the atmosphere, respectively; (d-f) SEM images of generator GTi after generating plasma using argon, nitrogen, and air as the atmosphere, respectively.

Regarding generator GTi, it is significantly more evident its degradation after an extended period of plasma generation. For the different discharge gases, the thin titanium layer seems to have suffered several cracks on the edges, and the curling of the electrode's layer is more pronounced, as shown in **Figure 3.2 (d-f)**. It is also noted an increase of nanoparticles spread over the dielectric surface and slight detachments of the electrode layer from the paper. The implications are again more severe in the air atmosphere, where even the finger-shaped filaments were eliminated.

GAu is the most affected and damaged after generating plasma for long periods (**Figure 3.3**). For instance, in every atmosphere, besides the electrode's curling, the gold layer is partially destroyed around the honeycomb's edges. Furthermore, the finger-shaped filaments are practically eliminated, and it is also possible to observe a detachment and multiple fractures of the gold layer all over the generator's surface. In all cases, it is also visible a re-deposition of gold nanoparticles throughout the dielectric's surface. As evidenced in Figure B 10, even with an inert atmosphere, such as argon, it is possible to observe this re-deposition of gold nanoparticles with the naked eye.

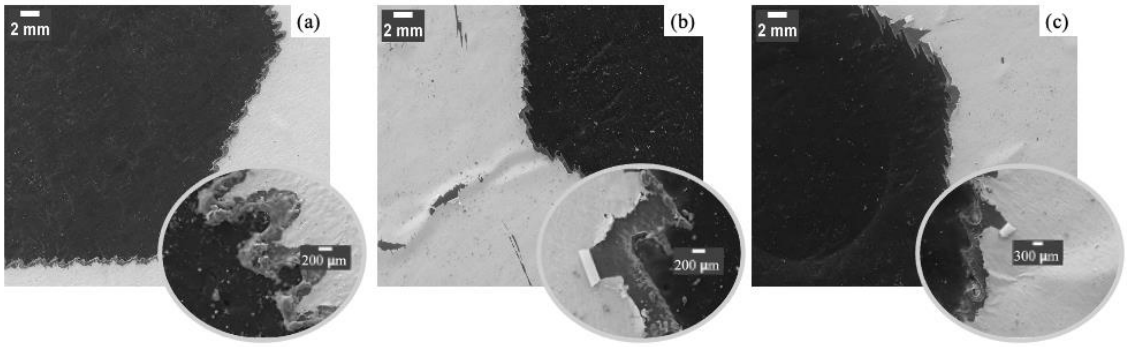

Figure 3.3 - (a-c) SEM images of generator GAu after generating plasma using argon, nitrogen, and air as the atmosphere, respectively.

An EDX elemental mapping on the dielectric and electrode surface was also performed in association with SEM imaging. In all cases, in the mapping of the dielectric surface, mainly carbon and oxygen are seen, which can be associated with the cellulosic nature of the substrate.

Although, for every atmosphere in GAl, GTi, and GAu, the presence of aluminum, titanium, and gold, respectively, on the dielectric surface results from the re-deposition of nanoparticles mentioned above. **Figure B 11,** is a clear example of the re-deposition of gold nanoparticles under an argon atmosphere, mentioned above.

Electrode erosion is the main limiting factor for the lifetime of these generators; on top of that it is also a source for undesired contamination. As mentioned, is section 2.1.2, one of the principal purposes of this thesis was to study the relevance of coating the aluminum layer with metals with higher resistance to corrosion and oxidation like gold and titanium and conclude whether they would bring any advantage or benefit to the generation of plasma. Through the results discussed in sections 3.3 and 3.4, it may be concluded that there were no advantages or improvements with these additional layers. In all atmospheres, generator GAl had the best performance and sustained plasma the best. Besides, it proved to be more resistant to surface degradation and maintained its properties after a prolonged period of plasma generation.

Fourier-transform infrared (FTIR) spectroscopy was also performed to analyze the surface of the generator chemically. FTIR is an analytical technique that enables identifying species and molecular groups present in a material through the absorption of radiation by the vibrational excitation of molecular bonds. Considering that the samples were analyzed before and after the generation of plasma, in this study, this technique is of particular interest since a change in the characteristic pattern of the absorption band can indicate a change in the composition of the surface of the generators.

Each generator was measured in two locations: on the surface of the honeycombs design (paper) and on top of the electrode surface (metal). However, there were no apparent differences in the spectra obtained for the electrode's surface, meaning the composition of the aluminum, gold, and titanium surfaces were not significantly altered after plasma generation; therefore, the results are not shown in this thesis. ATR-FTIR spectra of the surface of the honeycombs designs (cardboard) for generator GAl, GAu and GTi are shown in **Figure 3.4**, **Figure 3.5a** and **Figure 3.5b**, respectively.

Typically, the spectra would be normalized to the intensity of the band 2900 cm^{-1} due to its insensitivity to variations in the cellulose structure, crystallinity, and water content [46]. However, this normalization has not been carried out in the present thesis since there may still be remainders of the polymer adhesive layer that was not completely removed after the generators' patterning. Hence, there is a possible overlap at 2900 cm^{-1} of the absorption bands of cellulose and the low-density polyethylene (LDPE), which can mislead to wrong conclusions.

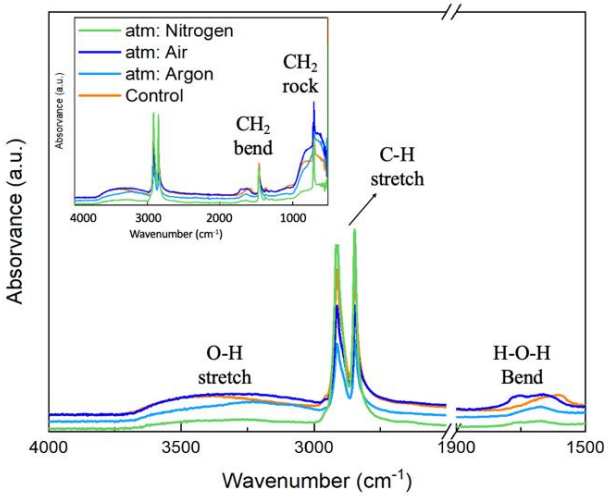

Figure 3.4 - ATR-FTIR spectra of GAl.

Similarly found by Kochetov R. *et al*., the spectra of the three generators reveal several characteristic absorption bands of low-density polyethylene (LDPE) [47]. It is possible to verify the presence of an aliphatic C-H stretching of methylene at 2930-2850 cm^{-1}, concealing the expected peak at 2900 cm^{-1} typically observed in cellulose-based substrates, the existence of a strong methylene (CH_2) band (1471 and 1462 cm^{-1}) and methyl (CH_3) band at 1376 cm^{-1}, indicative of a long-chain linear aliphatic structure, and the band at approximately 700 cm^{-1} which can be attributed to the CH_2 rocking vibrations (**Figures 3.4 and 3.5**).

Regarding generator GAl, the spectra in **Figure 3.4** reveal the characteristic absorption bands for cellulose and the hydrogen-bonded OH stretching at 3600-3200 cm^{-1} [48]. The presence of water in the samples can have a significant impact on the spectra obtained. This last-mentioned band can also be used to infer how water sorbs at the fiber surface as a result of water bounds directly to OH groups through hydrogen bonds. The peak at 3600 cm^{-1} is associated with water indirectly bonded to the OH groups via another water molecule [49]. Additionally, The peak at around 1650 cm^{-1} has been assigned to the O-H-O angle vibration of adsorbed water [49].

The data obtained for this generator suggest that there was weakly bonded water on the surface of the generator after plasma generation using both argon and air atmospheres. However, when using nitrogen as the discharge gas, the spectra are absent from the characteristic adsorbed water bands. These results may be explained by different elapsed times between the vacuum testing and the FTIR data acquisition. In the case of the first two gases, there may have been a partial recovery of water content by the samples, possibly due to a high timespan since they were extracted from the vacuum chamber until they were measured.

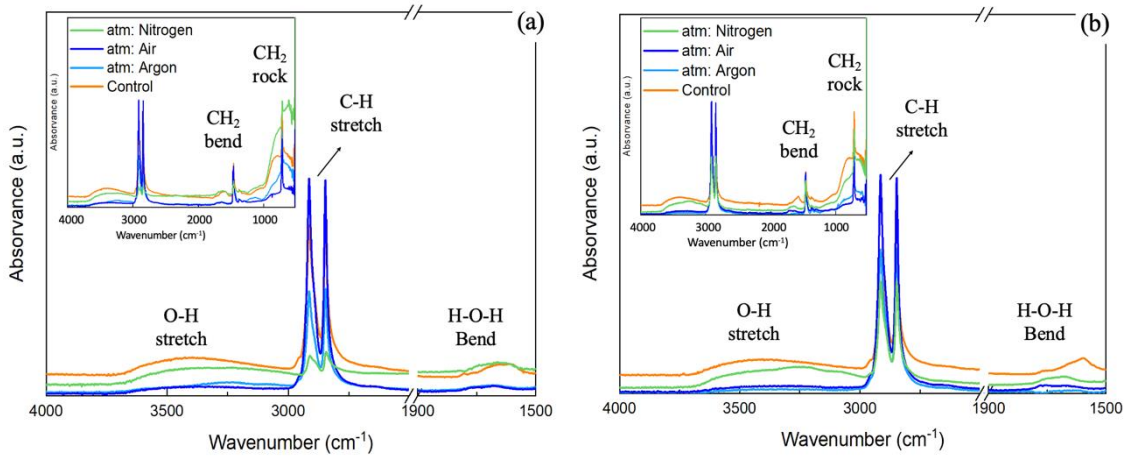

Figure 3.5 – ATR-FTIR spectra of (a) GAu, and (b) GTi

As for the case of generators GAu (**Figure 3.5a**) and GTi (**Figure 3.5b**), the characteristic absorption bands for cellulose can also be assigned. The reduced intensity of the characteristic adsorbed water bands indicates almost no water content in these cellulose fibers after plasma generation using these gases. Nonetheless, these results do not appear to be the case when using a nitrogen atmosphere. However, the samples may have partially recovered their water content when extracted from the vacuum chamber and measured, resulting in errors leading to non-conclusive results. Overall, there are no evident variations in the spectra obtained for the three different atmospheres. Thus, there were no significant changes on the surface of the generators after plasma generation.

3.5 Optical emission spectroscopy

As previously described in section 1, plasma is an exciting ionized gas that consists mainly of reactive atoms, ions, molecules, and radicals, which have a fundamental role in producing the so-

known RONS. It is due to their efficient delivery that plasma biologically affects cells and tissues. Thus, to identify the reactive species present in the plasma, optical emission spectroscopy was used.

OES is a qualitative technique that provides information about the elements present at a given sample and quantifies their intensity. In the plasma, molecules and radicals are excited mainly as a result of collisions with energetic electrons. When electrons transition between different energy levels, they emit radiation, producing spectral lines with well-defined wavelengths. Every element emits a series of specific optical emission lines corresponding to those electron transitions [50]. In the following discussion, three different aspects are going to be studied for each generator. One corresponds to an analysis of the reactive species present in the plasma generated with the various atmospheres. A second analysis concerning the influence of the applied rf power on the spectra obtained. Finally, an investigation of the influence of the applied pressure is going to be assessed. **Figures 3.5 (a-c)** depict the optical emission spectra generated by excited species in the different atmospheres using generator GAl.

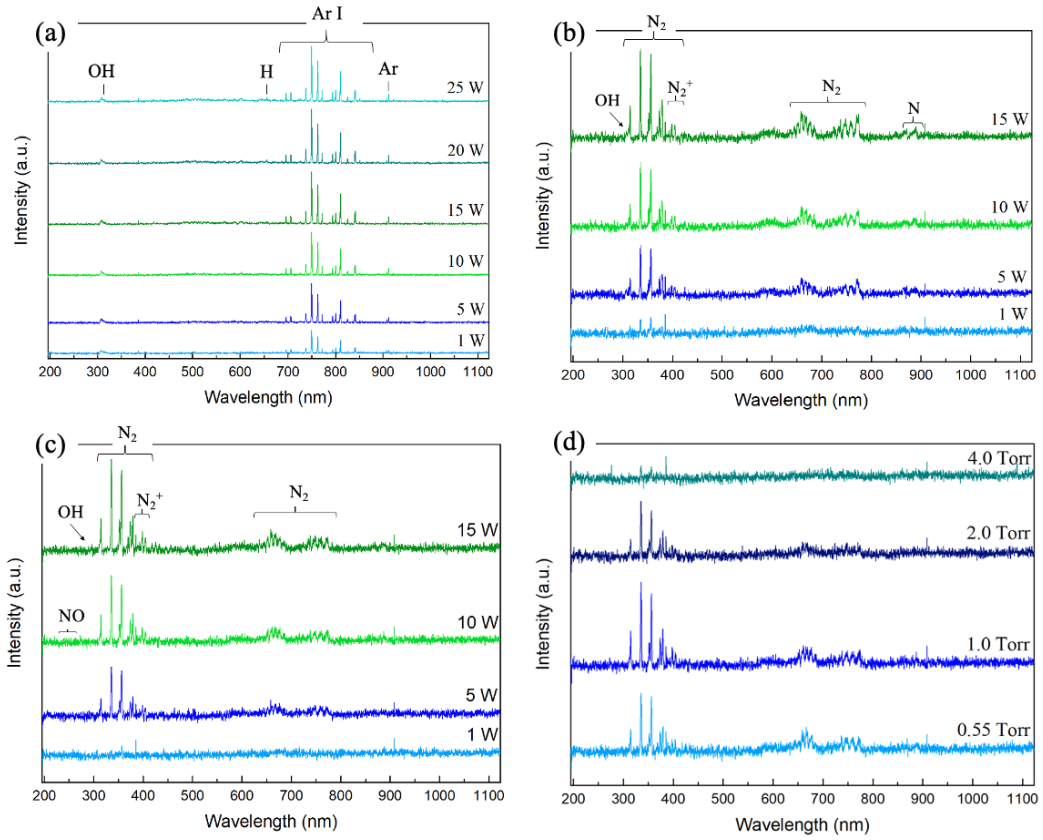

Figure 3.6 - (a-c) Optical emission spectra of generator GAl for the argon, nitrogen, and air atmospheres, respectively, under a pressure of 1 Torr; (d) Influence of pressure on the intensity of the spectral lines for generator GAl under air atmosphere applying 10 W.

As shown in **Figure 3.6a**, in argon plasma, in the visible and infrared region between 690 and 950 nm, one can easily observe various excited argon I atomic lines, as it is the major component of the atmosphere used [51]–[53]. The presence of hydroxyl radical (OH) at 307.8 nm and hydrogen (H) at around 650 nm may be attributed to the released adsorbed water molecules from the cellulose fibers, as confirmed by FTIR analyses [54]. This is because, using argon as the discharge gas, the excited electrons from argon dissociate water into hydrogen and hydroxyl radicals. **Equation 2** shows the potential primary mechanism of the dissociative excitation of the water molecule by the excited argon atoms Ar* [54], [55]:

$$Ar^* + H_2O \rightarrow Ar + OH^- + H^+ \quad (2)$$

Figures 3.6b and **3.6c** depict the spectra obtained for nitrogen and air discharges, respectively. For both cases, in the ultraviolet and visible region, between 200 and 450 nm, the key contributors to the spectrum are the emission of nitrogen molecules (N_2) around 300-410 nm and the molecular nitrogen ion (N_2^+) around 350-400 nm. Additionally, N_2 emission lines are presented at 600-800 nm, around 860-880 nm transitions of atomic nitrogen (N) may be identified, and OH radical is also observed at around 310 nm, possibly for the dissociation of the water molecules, adsorbed in the cellulose matrix, by the excited electrons present in the plasma. Besides nitrogen emission, air plasma may contain nitric oxide (NO) emission lines at 240-300 nm [52], [55], [56]. **Equation 3** demonstrates the possible pathway of water dissociation, whereas, the generation of NO in air plasma can be explained by **Equation 4** [57]–[59]

$$N_2^* + H_2O \rightarrow OH^- + H^+ + N_2 \quad (3)$$

$$N^+ + OH^- \rightarrow NO^- + H^+ \quad (4)$$

The intensity of the spectral lines at different pressure values is exemplified in **Figure 3.6d**, for plasma generation using air as the discharge gas. The remaining spectra for the other two atmospheres are presented in annex B, **Figures B 12a and B 12b.** For all discharge gases, the decrease of intensity of the spectral lines with the pressure could be explained by the reduction of the number of energetic electrons present at higher pressure, thereby the production rate of reactive species in the plasma is reduced [60]. On the other hand, as evidenced in **Figures 3.6 (a-c)**, increasing the applied rf power increases the spectral lines' intensity. A possible interpretation may be that a higher power density results in higher energy to produce more excited state levels of the electrons present in the discharge gas, hence increasing the concentration of active species.

Similar results were obtained for both generators GAu and GTi, using nitrogen and air as the discharge gases. As shown in **Figures B 13a**, **b** and **B 14a, b**, in both atmospheres, the principal identified species in the plasma are reactive nitrogen species, namely, N_2 (300-400 nm and 550-800 nm), N_2^+ (350-400 nm), and N (860-880 nm). The hydroxyl radical can also be found around 310 nm and in the case of air as the atmosphere, NO is present around 200-300 nm.

Figures 3.7a and **3.7b** illustrate the optical emission spectra generated by excited species using argon atmosphere for generators GAu and GTi, respectively. Both generators present the typical emission of argon I atomic lines at around 690-950 nm. Moreover, the dissociation of water into hydrogen and hydroxyl radical can also be observed. As mentioned in section 3.4.1, even in an inert atmosphere, there was a re-deposition of gold nanoparticles over the entire surface of the generator GAu. On top of that, it was the most susceptible to degradation after generating plasma over time. Therefore, can be assumed there was a reactive atmosphere when generating plasma and thus the existence of a gold emission line at 620 nm [61] and argon emission lines between 400 and 600 nm may be attributed [62] **(Figure 3.7a)**.

In the generator GTi, atomic titanium emission lines at around 460 and 520 nm can be identified (**Figure 3.7b**). The absence of these emission lines on the other two atmospheres can be explained by S. Yang *et al.*, where they reported that the energetic ions and neutral atomic and molecular nitrogen particles would react with the metal surface, reducing the sputtering yield from the titanium surface, therefore reducing titanium's emission lines [63]. The reactive species were identified and matched with NIST (National Institute of Standards and Technology) [64]. Notwithstanding, in all atmospheres, the propensity to increase the spectral lines' intensity with the applied rf power and decrease pressure is also noted for both generators (**Figures 3.7, B 13**, and **B 14**).

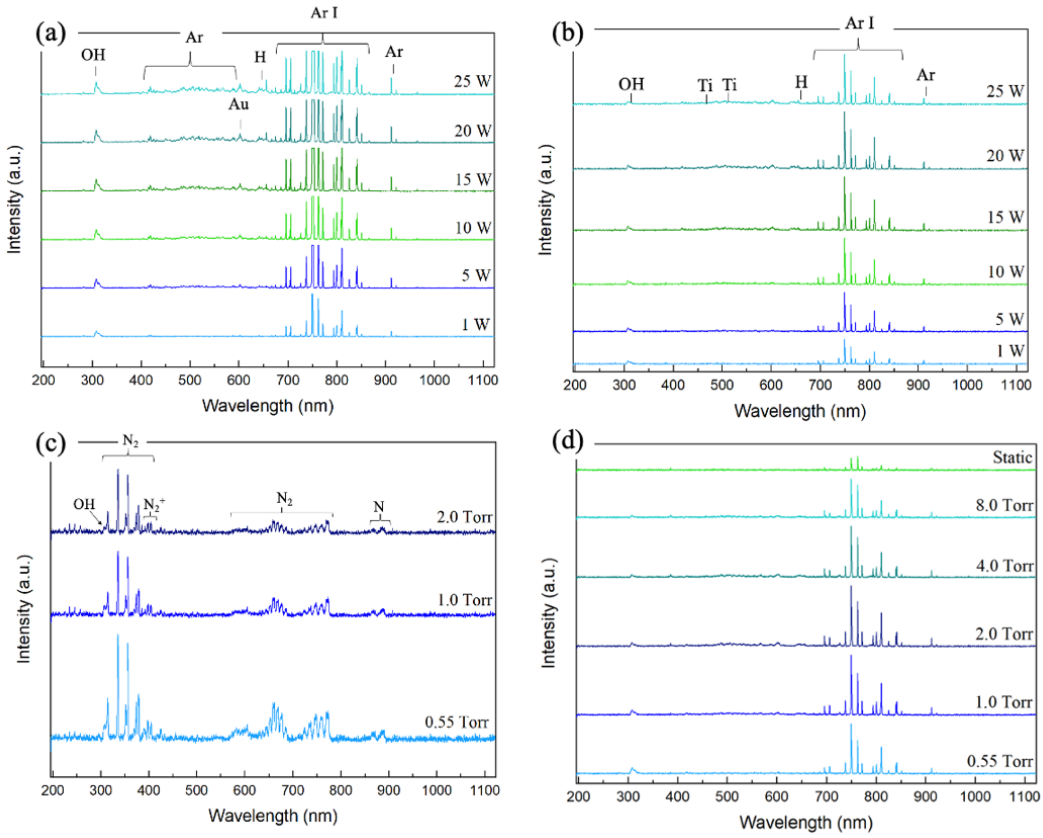

Figure 3.7 - Optical emission spectra of (a) generator GAu and (b) generator GTi, using argon atmosphere, under a pressure of 1 Torr. Influence of pressure on the intensity of the spectral lines for (c) generator GAu under nitrogen atmosphere, and (d) generator GTi under argon atmosphere, both applying 10 W.

Plasmas have proven to be highly beneficial for the medical and industrial sectors. As it is well known, the success of this novel technology is made through the indispensable and key enablers, the reactive oxygen and nitrogen species. The OES of these paper-based plasma generators indicates that many reactive species desirable in applications such as surface modification and biological decontamination are produced in the glow discharge. These include OH, excited N_2, NO, and argon metastables.

3.6 Miniaturization

Up to now, plasma-based generators frequently use rigid and bulky constituents, which cannot conform to irregularly shaped objects or access narrow areas where microbes might collect. For this purpose, scalable plasma designs are needed to develop safer and better-optimized plasma devices for human usage. Due to their reduced dimensions, these miniaturized paper-based plasma generators will represent an economic and ecological alternative for conventional technologies. They will have the potential to reduce healthcare-associated infections in varied urban and rural environments.

In such a manner, these generators' potential on a reduced scale was investigated. As a consequence of the better performance of generator GAl, the miniaturization tests were carried out only with this type of generator. They were reduced to half their scale using the patterning parameters mentioned in section 3.6 for GAl. In this study, the devices were operated for up to thirty minutes under an rf power of 5 W employing the three discharge gases studied earlier.

These tests' main objective was to evaluate the maximum pressure that the generators were capable of generating plasma over their entire surface area.

Figure 3.8 shows photographs of the chamber's interior for the three miniaturization tests. Under an air atmosphere (**Figure 3.8a**), the maximum pressure achieved was 2.5 Torr. At about 2.6 Torr, the glow discharge started to fade until there was no plasma generated at around 4.0 Torr. Similar results were obtained when using nitrogen as the discharge gas (**Figure 3.8b**). It reached a maximum pressure of 2.7 Torr, and plasma began to disappear around 3.0 Torr. The best results were achieved under an atmosphere of argon (**Figure 3.8c**). For thirty minutes, it sustained a stable discharge at a pressure of 8.0 Torr. Afterwards, the chamber's pressure was increased to its highest value, the static mode (<10,5 Torr), and the generator lasted an additional fifteen minutes.

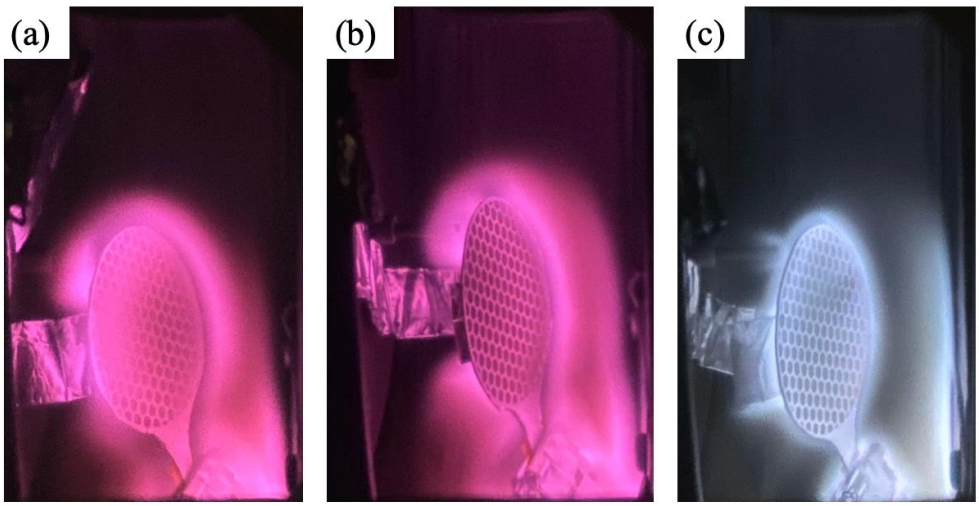

Figure 3.8 - Miniaturization tests: (a) air atmosphere; (b) nitrogen atmosphere; (c) argon atmosphere.

At the same time, OES analysis was performed. The spectra collected for the three atmospheres are presented in the annex section B **Figure B 15**. Similar results were obtained for these miniaturized devices. Essentially, the OES of these paper-based plasma generators includes OH, excited N_2, NO, and argon metastables.

Figure 3.9 shows the generators' temperature immediately after each test utilizing thermographic images. When generating plasma using air as the discharge gas (**Figure 3.9a**), the generator's average surface temperature after opening the chamber was 27.8 °C. As for the case of nitrogen plasma (**Figure 3.9b**), the generator reached an average temperature of 25.7 °C. Lastly, under an argon atmosphere (**Figure 3.9c**), the generator's surface reached an average of 38.6 °C. This increase of temperature compared to the other two atmospheres can be explained by the additional fifteen minutes of plasma generation that the generator under the argon atmosphere was exposed.

According to the DSC analysis, the paper's thermal degradation in use (LPC) starts only at about 250 ºC. With the results obtained by the thermographic images, one can conclude that these generators' proper function is not compromised, and neither is the degradation of these devices by temperature. Additionally, these generators achieve tolerable biological temperatures (T<40 ºC), meaning they can generate non-thermal plasmas (T<70 ºC). A possible explanation for these results could be due to the porous structure of LPC (P = 38,44 %) .Its permeability allows the flow of gas through its bulk volume providing fuel for the plasma and, simultaneously, can cool the paper [1].

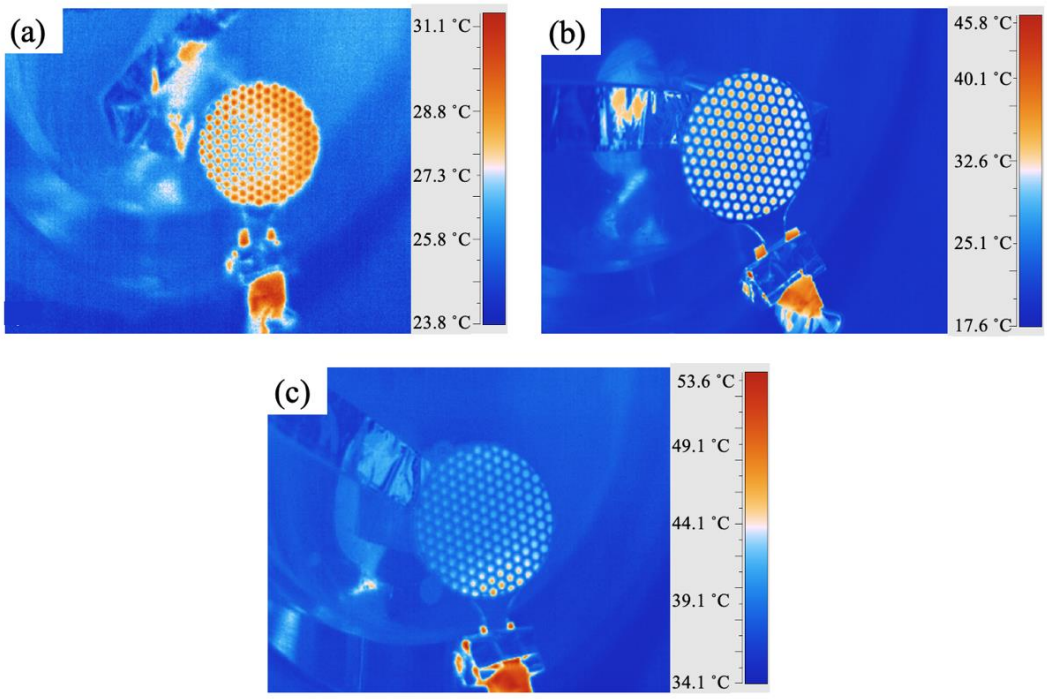

Figure 3.9 - Thermographic images obtained. (a) air atmosphere; (b) nitrogen atmosphere; (c) argon atmosphere.

3.7 Plasma confinement

In different fields such as food, biomedical and healthcare industries, nonthermal plasma is a promising decontamination approach with great advantages. One possible way of optimizing these decontamination processes without compromising the surrounding areas is through plasma confinement. In this work, plasma confinement was made through the implementation of an external magnetic field.

Similarly, to what happens in a magnetron sputtering system [65], a magnetic field was used to sustain the discharge in a close vicinity to the surface of the generator. A commercial magnet (**Figure B 16**) was placed on the generator's back and fixed to a glass support. The grounded lead was placed between the magnet and the generator's back electrode, while the power was applied to the generator's top electrode. **Figure 3.10a** illustrates the configuration used to confine the plasma. An additional image of the configuration and arrangement of the generator is presented in the annex section B, **Figure B 17**.

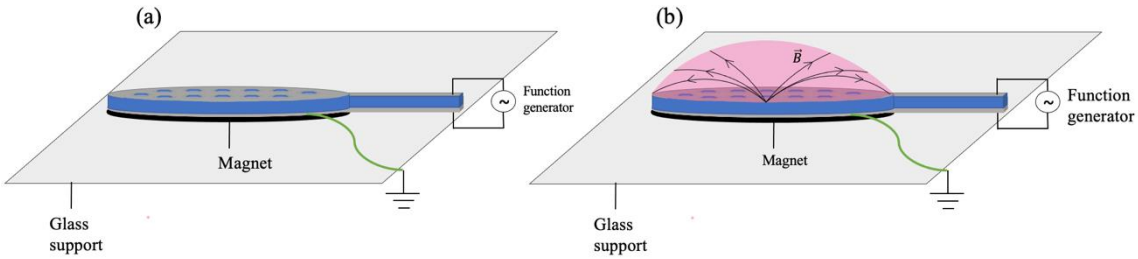

Figure 3.10 – (a) Schematic of the configuration used to confine the plasma. (b) Schematic of the magnetic field lines in the generator during plasma confinement using a magnet.

A preliminary test was carried out using generator GAl applying an rf power of 10 W and a pressure of 2 Torr and using argon as the discharge gas. The generator was operated for up to 15 minutes. With the confinement of the plasma using the commercial magnet, it is was possible to

observe a more dense and focused discharge, distributed in the close vicinity of the surface of the generator (**Figure 3.11a**). Due to the good results obtained, the same test was performed now using a miniaturized generator GAl. In the latter, as depicted in **Figure 3.11b**, even though it is not as perceptible as in the first case, the plasma discharge is also denser and in the immediate surrounding of the generator.

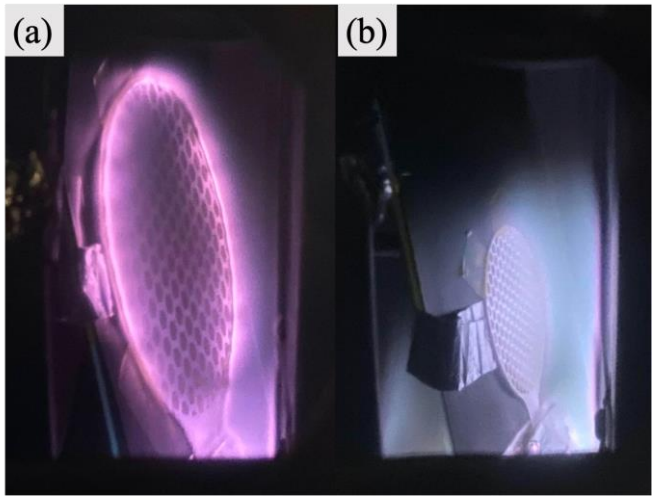

Figure 3.11 - Image obtained during the plasma confinement tests (a) normal generator; (b) miniaturized generator.

In order to evaluate the advantages of generating a more confined plasma, a comparison test was performed using the miniaturized generators. In this study, plasma was generated with and without the external magnetic field. It was used argon as the discharge gas and an rf power of a 10 W. The pressure values used were the same as in section 3.3.2 for the dependency on input power and pressure study. Before each increase, the pressure was kept constant for 5 min. **Figure 3.12** depicts both types of plasma generation. It is evident that using the commercial magnet (**Figure 3.12b**) plasma is denser and more concentrated in the immediate proximity of the generator's surface.

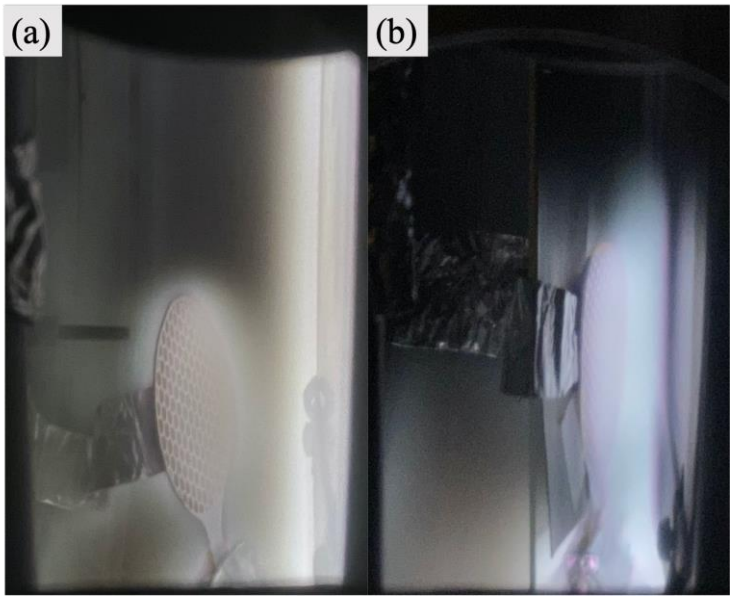

F**igure 3.12** - Images obtained during the comparison tests of plasma confinement: (a) without a magnet; (b) with a magnet.

The comparison shown in **Table 3.6** suggests that generating plasma using an external magnetic field not only is it able to confine plasma but also increase the dc bias potential considerably. As with any magnet, the magnetic material has a north and a south pole which are linked by magnetic field lines to complete a magnetic circuit. The commercial magnet placed behind the generator forms above its surface a magnetic field tunnel of magnetic lines (**Figure 3.10b**). These field lines trap electrons near the surface of the generator. As a result, electrons stay within the plasma for a longer time and hence the chance of making ionizing collisions is much higher. Thus, this increase of ionization leads to an increase in plasma density, therefore more reactive oxygen and nitrogen species are available for antimicrobial effects [66]–[69]

Table 3.6 - Dc bias values obtained for both types of plasma generation (P = 10 W; atmosphere: Ar).

Pressure (Torr)	**Plasma generation without magnet** dc bias (V)	**Plasma generation with magnet** dc bias (V)
0,55	[32-36]	[124-129]
1	[19-21]	[86-90]
2	[12-14]	[42-46]
4	[7-10]	[24-28]
8	[3-5]	[18-21]
>10,5	[1-2]	[14-18]

As a consequence of a more confined plasma in the generator's surface, it would be expected the heating of the device and thus a higher surface temperature. Although this was not the case. Instead, as shown in the thermographic image in **Figure 3.13**, the generator reached an average surface temperature of 30.2 ºC, for a plasma generation of 35 minutes. On another note, these generators achieve tolerable biological temperatures (T<40 ºC), representing a good approach to the generation of non-thermal plasmas (T<70 ºC).

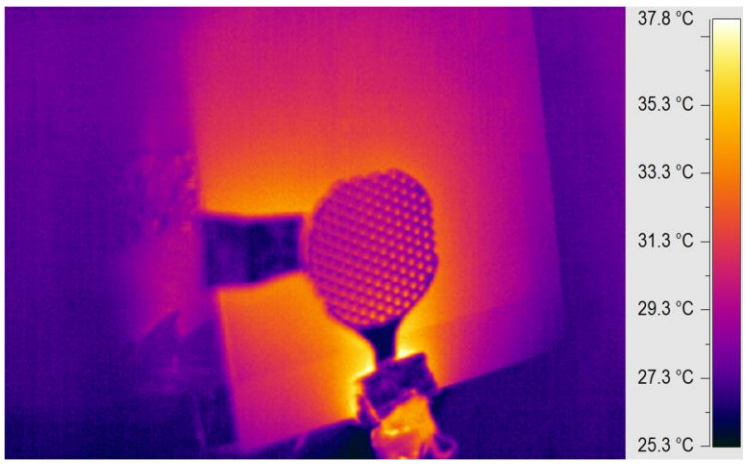

Figure 3.13 - Thermographic image obtained after plasma confinement.

4 Conclusion and Future Perspectives

The design adopted for this thesis consisted of a cellulose-based substrate commonly used in liquid packaging. This material is biodegradable, antiseptic, and composed of pressed cellulose fibers, acting as the dielectric material in the generator, and an aluminum sheet that forms the powered electrode. The generator is complete with a thin aluminum layer deposited on the back of these substrates forming the grounded electrode.

The experimental part of the plasma generation was divided into four main themes: (i) a comprehensive study on the influence of the operating conditions and parameters used; (ii) a chemical and morphological analyses of these devices before and after the generation of plasma; (iii) the identification of the reactive species present in the generated plasma; and finally (iv) miniaturization of these devices and consequent plasma generation studies. In addition to this, plasma confinement tests were carried out.

As mentioned before, electrode degradation is the main limiting factor for these generators' lifetime; on top of that, it is also a source for undesired contamination. For this reason, thin layers of metals with high inertness like gold and titanium were deposited on top of the aluminum sheet, and their relevance in decreasing surface degradation by plasma was assessed. Moreover, it was studied the influence of generating plasma using three different discharge gases, such as air, argon, and nitrogen, and the dependency on input power and pressure to ignite a discharge.

The results obtained demonstrated no improvements made with the addition of these layers of gold and titanium. In all atmospheres, the generator with a top electrode of aluminum (GAl) was the less degraded after long periods of plasma generation. The best results were achieved using lower pressure and under the argon atmosphere regarding the dependency on input power and pressure of these plasma generating devices. However, all types of generators could ignite a discharge using relatively low input rf power values. Overall, generator GAl is more effective in sustaining the plasma, regardless the atmosphere. These results show a promising future for generator GAl when generating plasma in atmospheric conditions.

Optical emission spectroscopy was used to identify the reactive species present in the plasma. The spectra obtained suggested that these fibrous, paper-like substrates could produce many reactive species desirable for biological decontamination and may be appropriate to produce plasmas capable of killing microbes.

These generators' potential on a reduced scale was investigated, and these tests were carried out using only generator GAl. The miniaturized generators reached the highest pressure of 8 Torr under an argon atmosphere, and in all cases presented tolerable biological temperatures ($T<40$ ºC), meaning they can generate non-thermal plasmas ($T<70$ ºC).

Finally, confining plasma by the miniaturized generators suggests that generating microplasma using an external magnetic field can confine the plasma and increase the dc bias potential considerably. As a result, there is an increase in the discharge gas's ionization; thus, more reactive species are available for possible antimicrobial effects.

Overall, these paper-based plasma generators have a vast potential in overcoming some of the drawbacks of plasma sterilization that remain. They are well-scalable, robust, and easy to adapt to complex geometries. Among all these advantages, their ability to effortlessly ignite a discharge is beyond doubt the most significant. Due to the outstanding results obtained, future research will focus on operating these devices in atmospheric conditions.

Atmospheric plasma sources require high voltages to generate plasma, not to mention their need to operate at pulsed or high frequencies to prevent an energetic equilibrium of the plasma, hence having a thermal character. Simultaneously, the necessity for high-voltage power supplies limits their application as portable devices. A current alternative approach to reducing the voltage amplitude is the utilization of piezoelectric crystals [69]. Briefly, employing a mechanical,

thermal, or electrical force alters their crystal structure, therefore changing their polarization magnitude. Prior works have demonstrated the generation of cold atmospheric plasma devices using piezoelectric transformers. Itoh *et al.* were the first to incorporate these electrical transformers in plasma sources [71]. In 2019, a study conducted by Johnson et al. aimed to characterize the electrical and optical properties of helium and argon plasma jets driven by piezoelectrical transformers [72]. Furthermore, Babij *et al.* record a novel approach to plasma-generating jets through a piezoelectric-powered capillary plasma system acting as an ionization source for ambient mass and ion mobility spectrometry [73]. More recently, Jinyu Yang and his research group reported time-resolved measurements of a free plasma jet formed off the surface of a commercial piezoelectric transformer actuated by a low-voltage AC input [70]. Despite the valuable discoveries made, there is still a lack of understanding of how plasma forms on the piezoelectric surface.

In this way, we also present a possible approach to this problem by generating microplasma using miniaturized generators. Because of their reduced dimensions, the utilization of low-power sources is possible. Due to the reactive species generated, the low-gas temperature, non-equilibrium character, and portability, these devices seem to have a vast potential in many low voltage driving applications and scientific areas.

References

[1] J. Xie, Q. Chen, P. Suresh, S. Roy, J. F. White, and A. D. Mazzeo, "Paper-based plasma sanitizers," *Proc. Natl. Acad. Sci. U. S. A.*, vol. 114, no. 20, pp. 5119–5124, 2017.

[2] A. K. Bose, C. L. Beaver, B. B. Narakathu, S. Rossbach, B. J. Bazuin, and M. Z. Atashbar, "Development of Flexible Microplasma Discharge Device for Sterilization Applications," *Proc. IEEE Sensors*, vol. 2018-Octob, pp. 1–4, 2018.

[3] X. Liao *et al.*, "Inactivation mechanisms of non-thermal plasma on microbes: A review," *Food Control*. 2017.

[4] W. A. Rutala and D. J. Weber, "Disinfection and Sterilization in Health Care Facilities: An Overview and Current Issues," *Infectious Disease Clinics of North America*. 2016.

[5] N. Ribeiro *et al.*, "A new era for sterilization based on supercritical CO2 technology," *Journal of Biomedical Materials Research - Part B Applied Biomaterials*. 2020.

[6] X. Li and M. Farid, "A review on recent development in non-conventional food sterilization technologies," *J. Food Eng.*, vol. 182, pp. 33–45, 2016.

[7] J. Ehlbeck *et al.*, "Low temperature atmospheric pressure plasma sources for microbial decontamination," *J. Phys. D. Appl. Phys.*, vol. 44, no. 1, 2011.

[8] M. Laroussi, "Plasma Medicine: A Brief Introduction," *Plasma*, vol. 1, no. 1, pp. 47–60, 2018.

[9] T. von Woedtke, S. Reuter, K. Masur, and K. D. Weltmann, "Plasmas for medicine," *Phys. Rep.*, vol. 530, no. 4, pp. 291–320, 2013.

[10] N. De Geyter and R. Morent, "Nonthermal plasma sterilization of living and nonliving surfaces," *Annu. Rev. Biomed. Eng.*, vol. 14, no. 1, pp. 255–274, 2012.

[11] S. Samal, "Thermal plasma technology: The prospective future in material processing," *J. Clean. Prod.*, vol. 142, no. 4, pp. 3131–3150, 2017.

[12] K. D. Weltmann and T. Von Woedtke, "Plasma medicine - Current state of research and medical application," *Plasma Phys. Control. Fusion*, vol. 59, no. 1, 2017.

[13] M. Laroussi, "Low-temperature plasmas for medicine?," *IEEE Trans. Plasma Sci.*, vol. 37, no. 6 PART 1, pp. 714–725, 2009.

[14] K. D. Weltmann, K. Fricke, M. Stieber, R. Brandenburg, T. Von Woedtke, and U. Schnabel, "New nonthermal atmospheric-pressure plasma sources for decontamination of human extremities," *IEEE Trans. Plasma Sci.*, vol. 40, no. 11, pp. 2963–2969, 2012.

[15] J. L. Zimmermann, T. Shimizu, V. Boxhammer, and G. E. Morfill, "Disinfection through different textiles using low-temperature atmospheric pressure plasma," *Plasma Process. Polym.*, 2012.

[16] M. Laroussi, "Low temperature plasma-based sterilization: Overview and state-of-the-art," *Plasma Processes and Polymers*. 2005.

[17] G. Isbary *et al.*, "Cold atmospheric plasma devices for medical issues," *Expert Rev. Med. Devices*, vol. 10, no. 3, pp. 367–377, 2013.

[18] F. Iza *et al.*, "Microplasmas: Sources, particle kinetics, and biomedical applications," *Plasma Processes and Polymers*. 2008.

[19] R. Brandenburg, "Dielectric barrier discharges: Progress on plasma sources and on the understanding of regimes and single filaments," *Plasma Sources Science and Technology*. 2017.

[20] U. Kogelschatz, "Dielectric-barrier discharges: Their History, Discharge Physics, and Industrial Applications," *Plasma Chemistry and Plasma Processing*. 2003.

[21] X. Zhao *et al.*, "Fabrication of Transparent Paper-Based Flexible Thermoelectric Generator for Wearable Energy Harvester Using Modified Distributor Printing Technology," *ACS Appl. Mater. Interfaces*, vol. 11, no. 10, pp. 10301–10309, 2019.

[22] G. H.-Q. Lateral and O. Bulk, "JMEMS Letters," *J. Microelectromechanical Syst.*, vol. 21, no. 2, pp. 253–255, 2012.

[23] M. Laroussi, X. Lu, and M. Keidar, "Perspective: The physics, diagnostics, and applications of atmospheric pressure low temperature plasma sources used in plasma medicine," *J. Appl. Phys.*, 2017.

[24] M. Laroussi, "Sterilization of contaminated matter with an atmospheric pressure plasma," *IEEE Trans. Plasma Sci.*, 1996.

[25] G. E. Morfill, T. Shimizu, B. Steffes, and H. U. Schmidt, "Nosocomial infections - A new approach towards preventive medicine using plasmas," *New J. Phys.*, 2009.

[26] B. G. Dasan, M. Mutlu, and I. H. Boyaci, "Decontamination of Aspergillus flavus and Aspergillus parasiticus spores on hazelnuts via atmospheric pressure fluidized bed plasma reactor," *Int. J. Food Microbiol.*, 2016.

[27] S. Deng, R. Ruan, C. K. Mok, G. Huang, X. Lin, and P. Chen, "Inactivation of Escherichia coli on almonds using nonthermal plasma," *J. Food Sci.*, 2007.

[28] X. Liu, F. Hong, Y. Guo, J. Zhang, and J. Shi, "Sterilization of staphylococcus aureus by an atmospheric non-thermal plasma jet," *Plasma Sci. Technol.*, 2013.

[29] H. I. Yong *et al.*, "Evaluation of pathogen inactivation on sliced cheese induced by encapsulated atmospheric pressure dielectric barrier discharge plasma," *Food Microbiol.*, 2015.

[30] P. Muranyi, J. Wunderlich, and M. Heise, "Influence of relative gas humidity on the inactivation efficiency of a low temperature gas plasma," *J. Appl. Microbiol.*, 2008.

[31] M. Laroussi, D. A. Mendis, and M. Rosenberg, "Plasma interaction with microbes," *New J. Phys.*, 2003.

[32] S. G. Joshi *et al.*, "Nonthermal dielectric-barrier discharge plasma-induced inactivation involves oxidative DNA damage and membrane lipid peroxidation in Escherichia coli," *Antimicrob. Agents Chemother.*, 2011.

[33] O. Lunov *et al.*, "The interplay between biological and physical scenarios of bacterial death induced by non-thermal plasma," *Biomaterials*, 2016.

[34] D. A. Mendis, M. Rosenberg, and F. Azam, "A note on the possible electrostatic disruption of bacteria," *IEEE Trans. Plasma Sci.*, 2000.

[35] J. L. Zimmermann, T. Shimizu, H. U. Schmidt, Y. F. Li, G. E. Morfill, and G. Isbary, "Test for bacterial resistance build-up against plasma treatment," *New J. Phys.*, 2012.

[36] Stora Enso, "No Title." [Online]. Available: http://www.storaenso.com/.

[37] T. C. Hales, "The honeycomb conjecture," *Discret. Comput. Geom.*, 2001.

[38] National Library of Medicine, "Cellulose." [Online]. Available: https://pubchem.ncbi.nlm.nih.gov/compound/CELLULOSE.

[39] H. A. Foner and N. Adan, "The Characterization of Papers by X-Ray Diffraction (XRD): Measurement of Cellulose Crystallinity and Determination of Mineral Composition," *J. Forensic Sci. Soc.*, 1983.

[40] C. Li, F. Huang, J. Wang, X. Liang, S. Huang, and J. Gu, “Effects of partial replacement of carbon black with nanocrystalline cellulose on properties of natural rubber nanocomposites,” *J. Polym. Eng.*, 2018.

[41] C. O. Ayieko, R. J. Musembi, A. A. Ogacho, B. O. Aduda, B. M. Muthoka, and P. K. Jain, “Controlled Texturing of Aluminum Sheet for Solar Energy Applications,” *Adv. Mater. Phys. Chem.*, 2015.

[42] K. Deshmukh *et al.*, *Dielectric Spectroscopy*, vol. 2. Elsevier Inc., 2017.

[43] M. Laroussi, I. Alexeff, J. P. Richardson, and F. F. Dyer, “The resistive barrier discharge,” *IEEE Trans. Plasma Sci.*, vol. 30, no. 1 I, pp. 158–159, 2002.

[44] M. Parker and R. Kenneth Marcus, “Investigation of dielectric sample atomization and electrical characteristics in a radio frequency glow discharge source,” *Spectrochim. Acta Part B At. Spectrosc.*, vol. 50, no. 4–7, pp. 617–638, 1995.

[45] M. J. Kushner, “Monte-Carlo simulation of electron properties in rf parallel plate capacitively coupled discharges,” *J. Appl. Phys.*, vol. 54, no. 9, pp. 4958–4965, 1983.

[46] L. Pereira, D. Gaspar, D. Guerin, A. Delattre, E. Fortunato, and R. Martins, “The influence of fibril composition and dimension on the performance of paper gated oxide transistors,” *Nanotechnology*, 2014.

[47] R. Kochetov, T. Christen, and F. Gullo, “FTIR analysis of LDPE and XLPE thin samples pressed between different protective anti-Adhesive films,” *ICEMPE 2017 - 1st Int. Conf. Electr. Mater. Power Equip.*, pp. 49–52, 2017.

[48] J. Coates, “Interpretation of Infrared Spectra, A Practical Approach,” in *Encyclopedia of Analytical Chemistry*, 2006.

[49] A. M. Olsson and L. Salmén, “The association of water to cellulose and hemicellulose in paper examined by FTIR spectroscopy,” *Carbohydr. Res.*, vol. 339, no. 4, pp. 813–818, 2004.

[50] HITACHI, “What is Optical Emission Spectroscopy (OES) ?” .

[51] K. E. Evdokimov, M. E. Konischev, V. F. Pichugin, and Z. Sun, “Study of argon ions density and electron temperature and density in magnetron plasma by optical emission spectroscopy and collisional-radiative model,” *Resour. Technol.*, 2017.

[52] W. Jiang, J. Tang, Y. Wang, W. Zhao, and Y. Duan, “Characterization of argon direct-current glow discharge with a longitudinal electric field applied at ambient air,” *Sci. Rep.*, 2014.

[53] A. Sarani, A. Y. Nikiforov, and C. Leys, “Atmospheric pressure plasma jet in Ar and Ar/ H2 O mixtures: Optical emission spectroscopy and temperature measurements,” *Phys. Plasmas*, vol. 17, no. 6, pp. 0–8, 2010.

[54] S. Meiyazhagan, S. Yugeswaran, P. V. Ananthapadmanabhan, P. R. Sreedevi, and K. Suresh, “Relative Potential of Different Plasma Forming Gases in Degradation of Rhodamine B Dye by Microplasma Treatment and Evaluation of Reuse Prospectus for Treated Water as Liquid Fertilizer,” *Plasma Chem. Plasma Process.*, 2020.

[55] P. Lukes and B. R. Locke, “Plasmachemical oxidation processes in a hybrid gas-liquid electrical discharge reactor,” *J. Phys. D. Appl. Phys.*, 2005.

[56] F. do Nascimento, S. Moshkalev, and M. Machida, “Changes in Properties of Dielectric Barrier Discharge Plasma Jets for Different Gases and for Insulating and Conducting Transfer Plates,” *Brazilian J. Phys.*, 2017.

[57] X. L. Deng, A. Y. Nikiforov, P. Vanraes, and C. Leys, “Direct current plasma jet at

atmospheric pressure operating in nitrogen and air," *J. Appl. Phys.*, 2013.

[58] A. Fridman, *Plasma chemistry*. 2008.

[59] H. S. Uhm, "Generation of various radicals in nitrogen plasma and their behavior in media," *Phys. Plasmas*, vol. 22, no. 12, 2015.

[60] A. Qayyum *et al.*, "Characterization of argon plasma by use of optical emission spectroscopy and Langmuir probe measurements," *Int. J. Mod. Phys. B*, 2003.

[61] N. Ahmed, R. Ahmed, and M. A. Baig, "Analytical Analysis of Different Karats of Gold Using Laser Induced Breakdown Spectroscopy (LIBS) and Laser Ablation Time of Flight Mass Spectrometer (LA-TOF-MS)," *Plasma Chem. Plasma Process.*, 2018.

[62] X. Dong *et al.*, "Emission spectroscopy of Ar + H2 + C7H8 plasmas: C7H8 flow rate dependence and pressure dependence," in *Journal of Physics: Conference Series*, 2014.

[63] S. Yang, M. Kitchen, Q. Luo, D. N. Ievlev, and K. E. Cooke, "Effect of Nitriding Time on the Structural Evolution and Properties of Austenitic Stainless Steel Nitrided Using High Power Pulsed DC Glow Discharge Ar/N2 Plasma," *J. Coat. Sci. Technol.*, vol. 3, no. 2, pp. 62–74, 2016.

[64] NIST: National Institute of Standards and Technology, "Atomic Spectra Database." .

[65] C. A. Bishop, "Magnetron Sputtering Source Design and Operation," *Vac. Depos. Onto Webs, Film. Foils*, pp. 371–399, 2015.

[66] J. Musil, J. Vlcek, and P. Baroch, "Magnetron Discharges for Thin Films Plasma Processing," *Mater. Surf. Process. by Dir. Energy Tech.*, pp. 67–110, 2006.

[67] M. S. Kandelousi and D. D. Ganji, "Flow heat transfer in the presence of a magnetic field," *Hydrothermal Anal. Eng. Using Control Vol. Finite Elem. Method*, pp. 77–176, 2015.

[68] T. J. Dolan, *Plasma Confinement*, no. November. 1982.

[69] W. L. Johnson, "Electrostatically-Shielded Inductively-Coupled RF Plasma Sources," *High Density Plasma Sources*, pp. 100–148, 1995.

[70] J. Yang, S. K. Im, and D. B. Go, "Time-resolved characterization of a free plasma jet formed off the surface of a piezoelectric crystal," *Plasma Sources Sci. Technol.*, 2020.

[71] K. Teranishi, S. Suzuki, and H. Itoh, "Observation of Light Emission in Silent Discharge Using Piezoelectric Transformer," *IEEJ Trans. Fundam. Mater.*, 2002.

[72] M. J. Johnson, D. R. Boris, T. B. Petrova, and S. G. Walton, "Characterization of a compact, low-cost atmospheric-pressure plasma jet driven by a piezoelectric transformer," *IEEE Trans. Plasma Sci.*, 2019.

[73] M. Babij, Z. W. Kowalski, K. Nitsch, J. Silberring, and T. Gotszalk, "Atmospheric pressure plasma jet with high-voltage power supply based on piezoelectric transformer," *Rev. Sci. Instrum.*, 2014.

[74] S. Dasgupta *et al.*, "Printed and electrochemically gated, high-mobility, inorganic oxide nanoparticle FETs and their suitability for high-frequency applications," *Adv. Funct. Mater.*, 2012.

Annexes

Annex A: Materials and Methods

This annex provides additional information concerning the Materials and methods section.

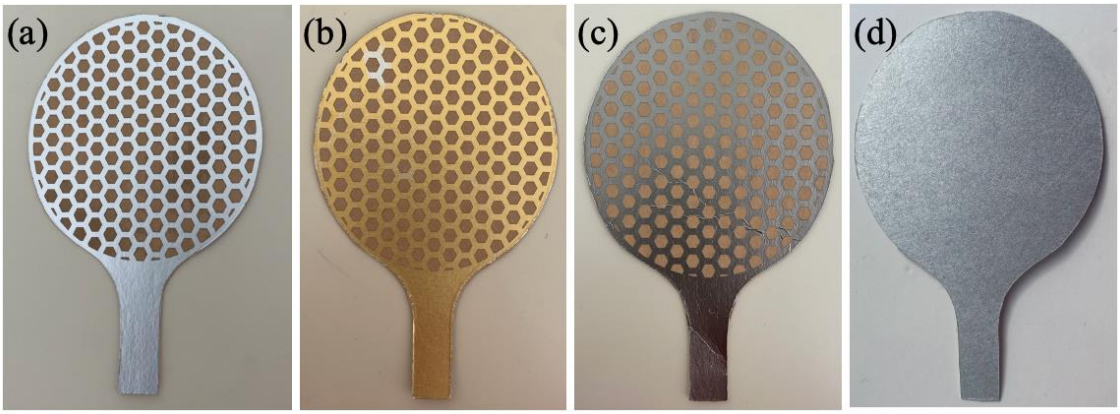

Figure A 1 - Paper-based plasma generators with different electrode types: (a) GAl: with top electrode of aluminum; (b) GAu: with top electrode of aluminum with a thin layer of gold; (c) GTi: with top electrode of aluminum with a thin layer of titanium; (d) bottom electrode for the three types of generators: thin layer of aluminum.

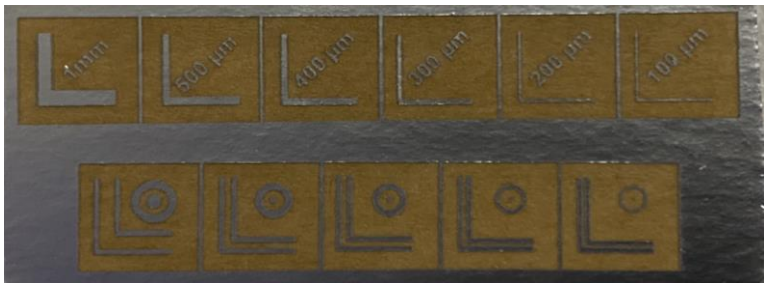

Figure A 2 - Resolution analyses of the miniaturization study.

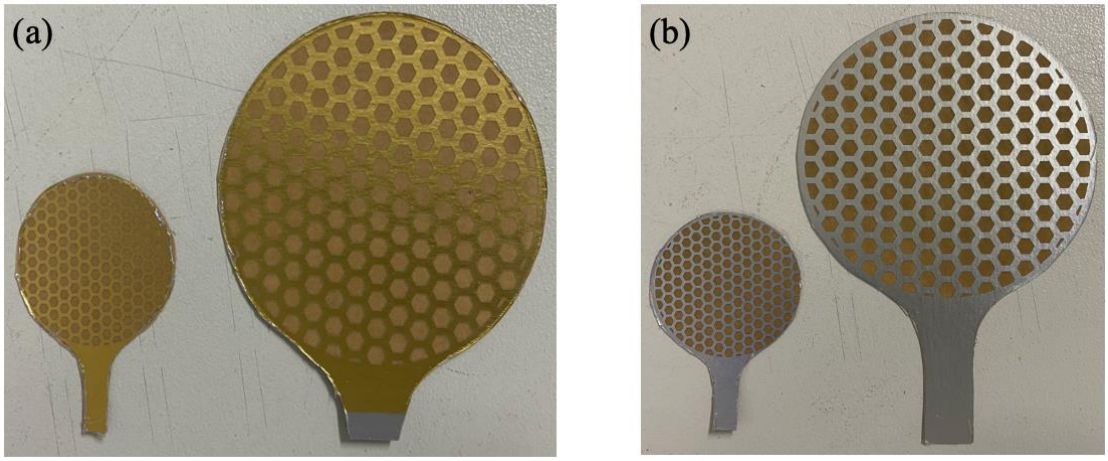

Figure A 3 - Comparison between a normal generator and a miniaturized one: (a) Generator with gold electrodes; (b) Generator with aluminum electrodes.

Annex B: Results and Discussion

In this section will be presented supplementary information regarding the Results and Discussion section.

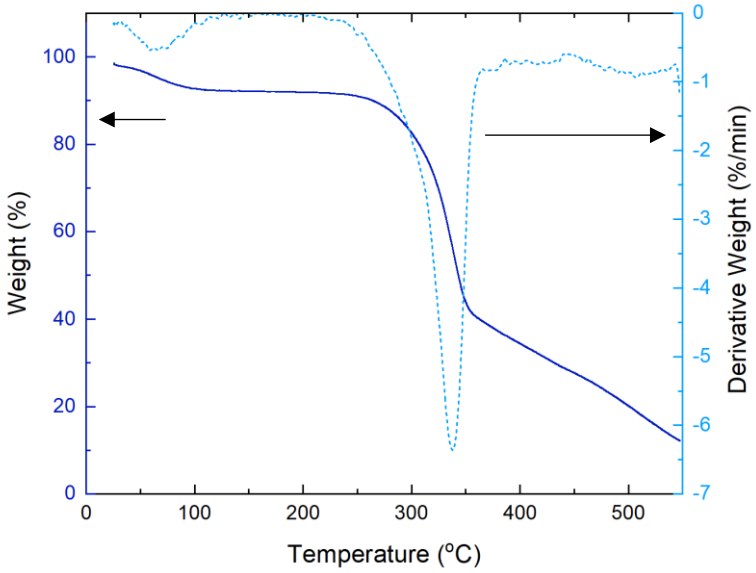

Figure B 1 - Thermal analysis of the liquid packaging cardboard. The thermogravimetric analysis is represented in the left yy axis, and derivate weight is represented in the right yy axis.

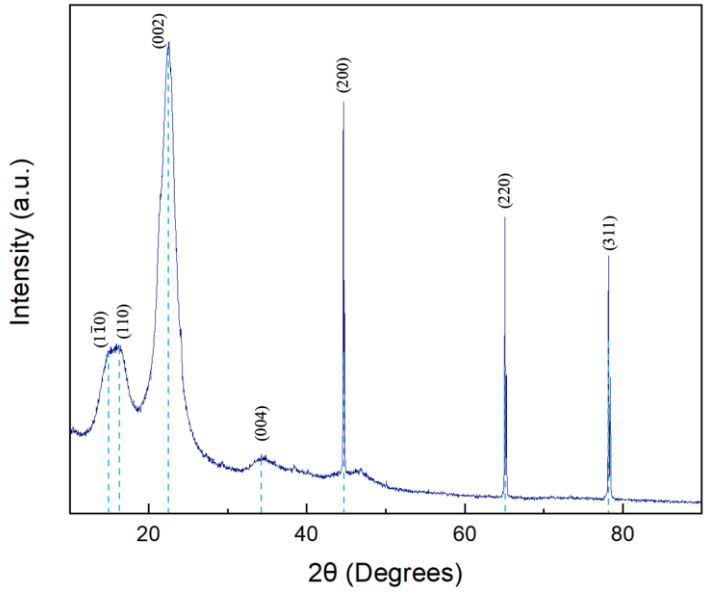

Figure B 2 - XRD diffractogram for the liquid packaging cardboard.

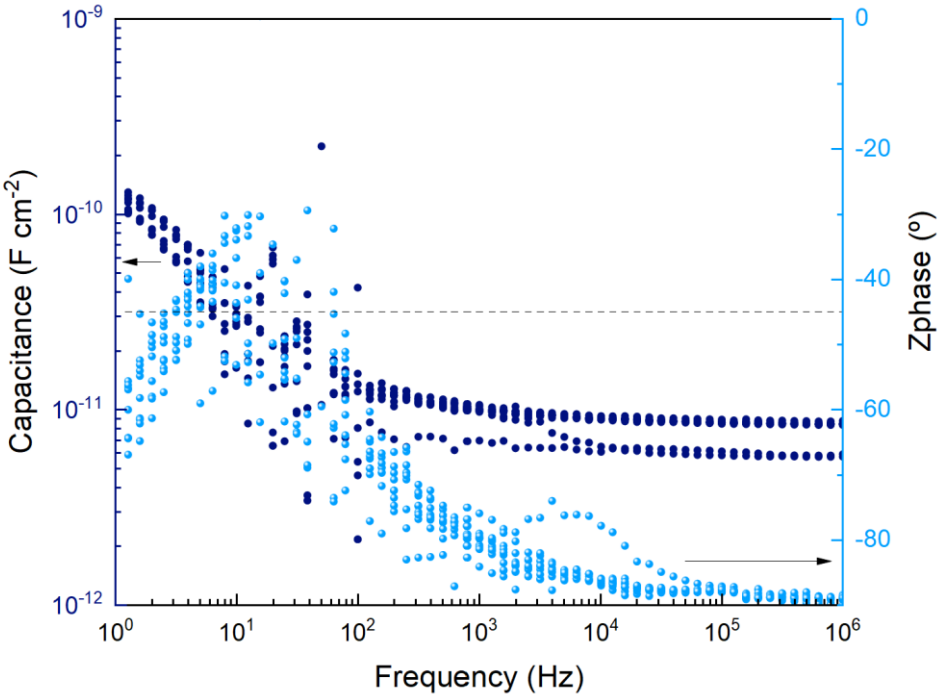

Figure B 3 - Eletrochemical impedance spectroscopy: Capacitance and phase variation with frequency.

The capacitance calculated for the impedance spectroscopy spectra is presented in **Equation B1**:

$$C = -\frac{Z_{Imag}}{\omega \times |Z|^2} \qquad \text{Equation B1}$$

Where Z_{imag} is the imaginary part of the impedance and ω is the angular frequency ($\omega = 2\pi f$) [74].

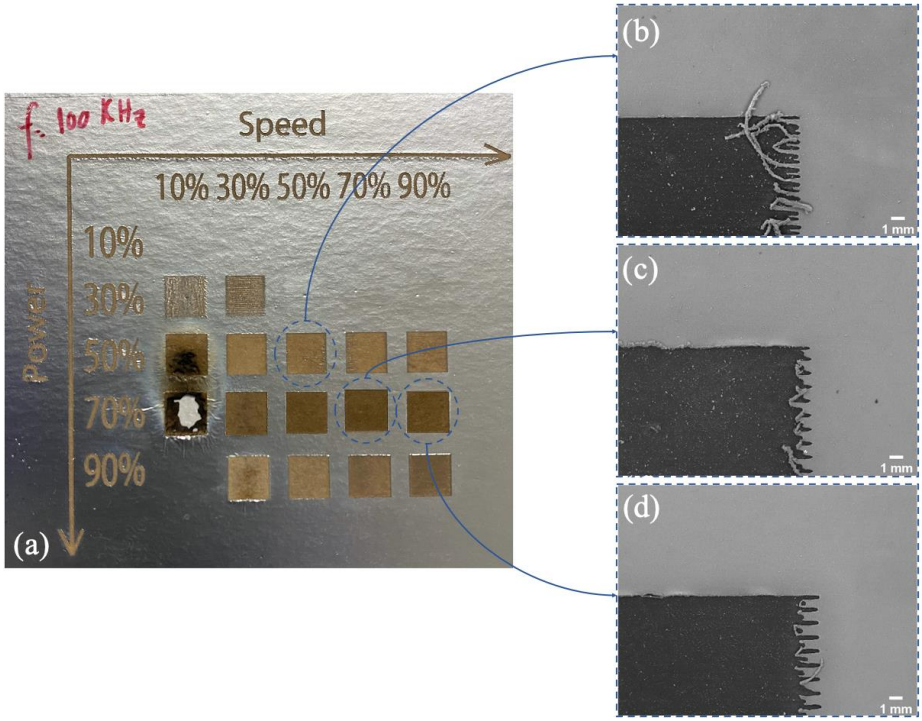

Figure B 4 - Aluminum electrode: (a) matrix of Power vs Speed with frequency 100 kHz; SEM images of the three best engraved squares: (b) P=50% and S=50%; (c) P=70% and S=70%; (d) P=70% and S=90%.

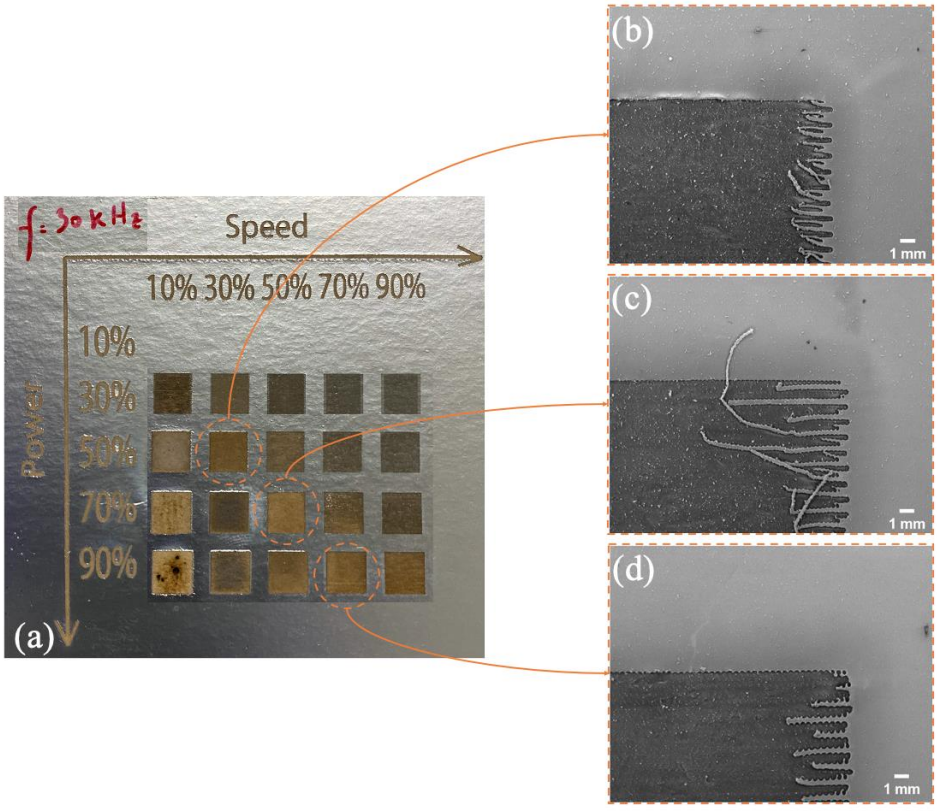

Figure B 5 - Aluminum electrode: (a) matrix of Power vs Speed with frequency 30 kHz; SEM images of the three best engraved squares: (b) P=50% and S=30%; (c) P=70% and S=50%; (d) P=90% and S=70%.

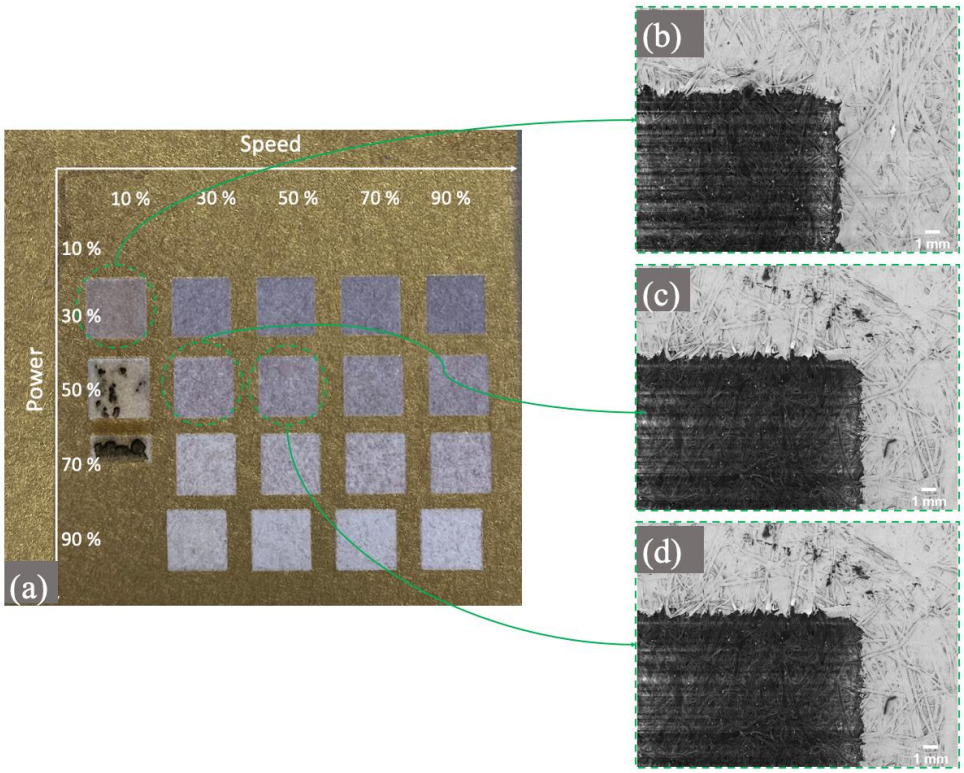

Figure B 6 - Gold electrode: (a) matrix of Power vs Speed with frequency 100 kHz; SEM images of the three best engraved squares: (b) P=30% and S=10%; (c) P=50% and S=30%; (d) P=50% and S=50%.

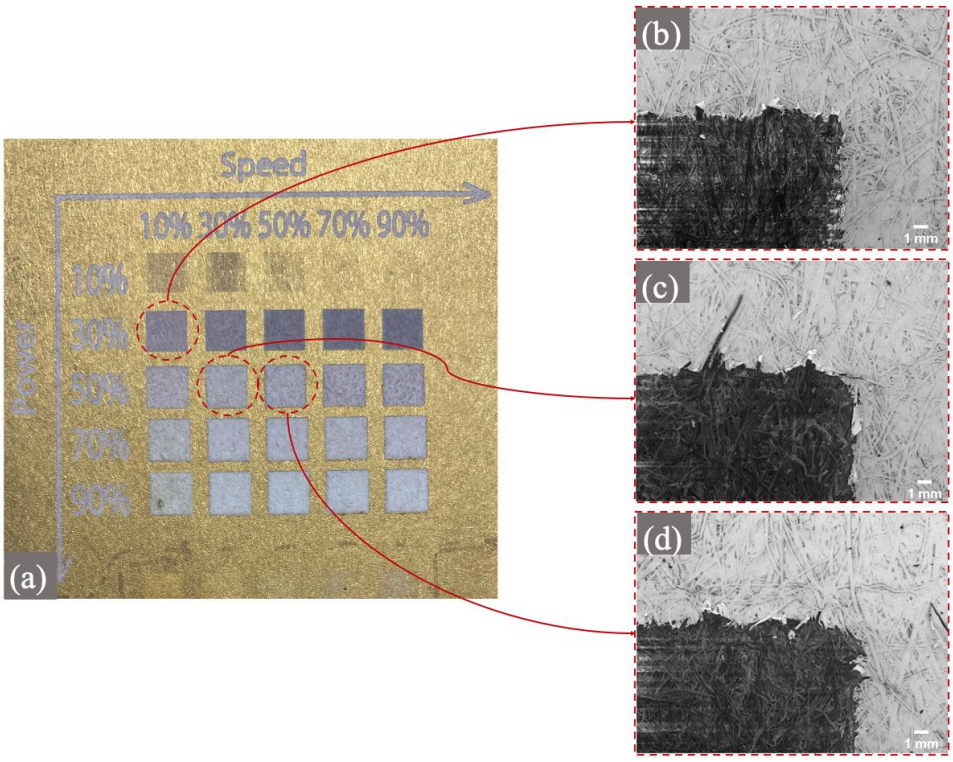

Figure B 7 - Gold electrode: (a) matrix of Power vs Speed with frequency 30 kHz; SEM images of the three best engraved squares: (b) P=30% and S=10%; (c) P=50% and S=30%; (d) P=50% and S=50%.

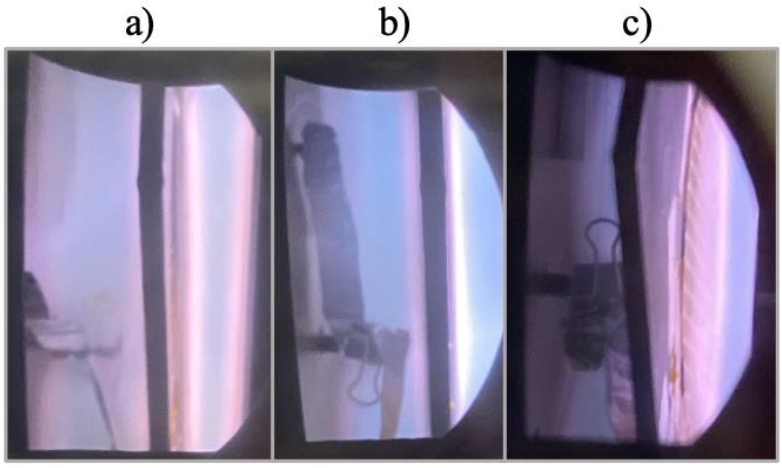

Figure B 8 - Paper-based generators generating plasma: a) Generator GTi; b) Generator GAl; c) Generator GAu.

Table B 1 - Matrix of Power vs Pressure for the generator GAl using an argon atmosphere.

Pressure (Torr) \ Power (W)	1	5	10	15	20	25
0,55	23 V	61 V	80 V	116 V	138 V	155 V
1	13 V	43 V	57 V	86 V	107 V	126 V
2	7 V	25 V	35 V	49 V	61 V	84 V
4	5 V	15 V	20 V	28 V	33 V	44 V
8		10 V	15 V	18 V	20 V	21 V

Table B 2 - Matrix of Power vs Pressure for the generator GAu using an argon atmosphere.

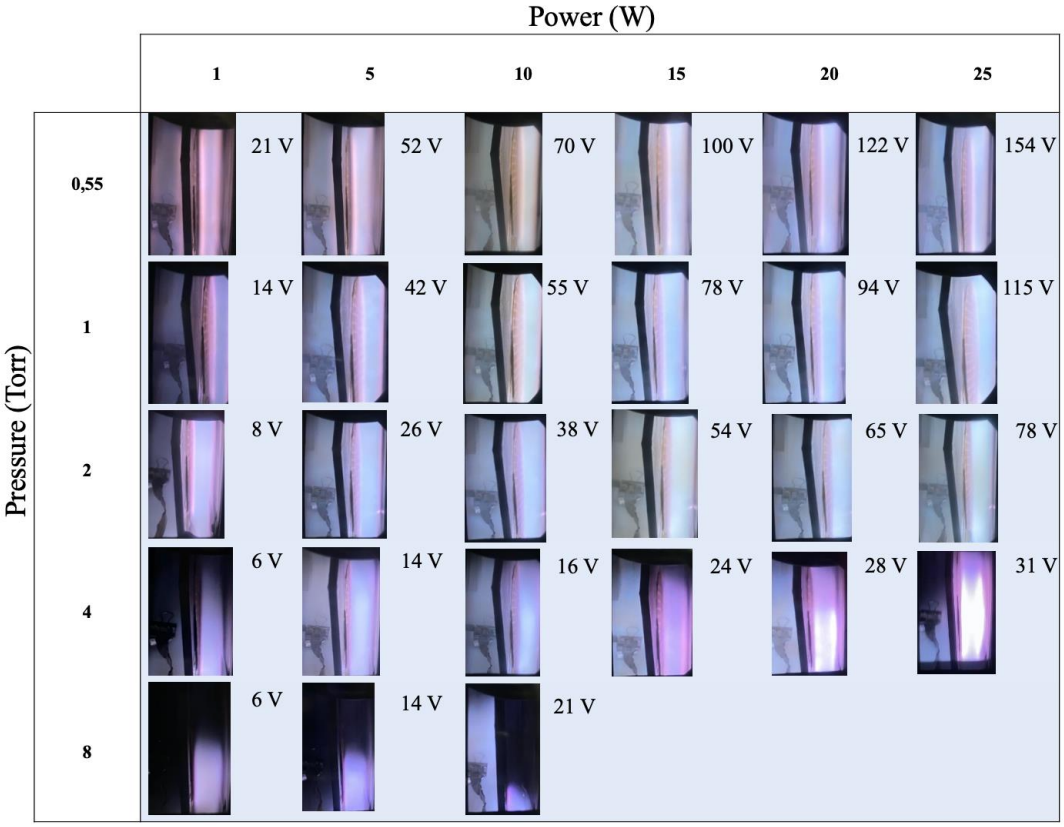

Table B 3 - Matrix of Power vs Pressure for the generator GAl using a nitrogen atmosphere.

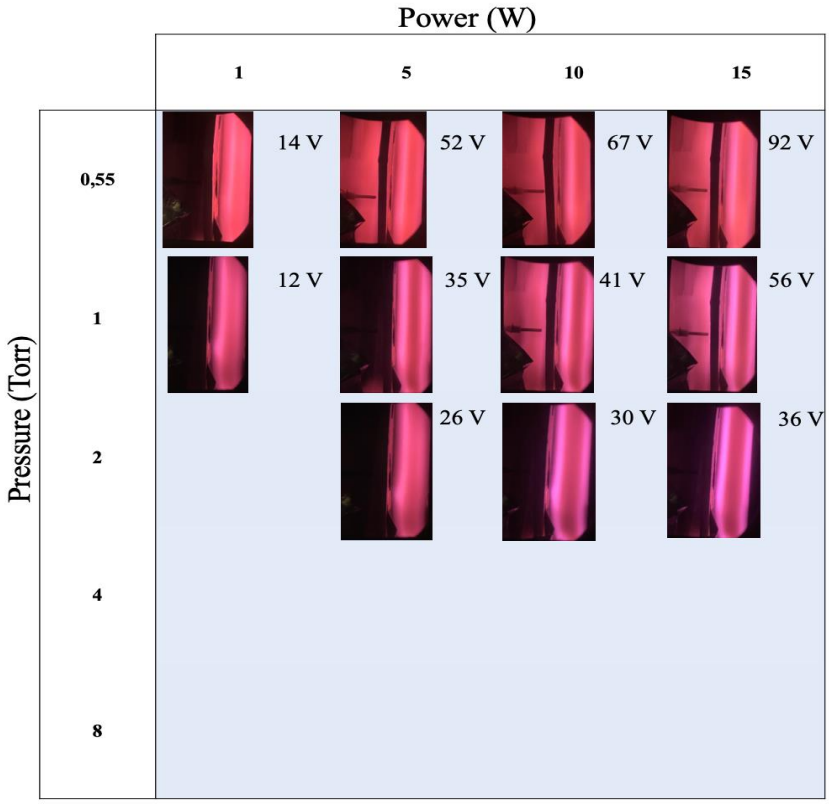

Table B 4 - Matrix of Power vs Pressure for the generator GTi using a nitrogen atmosphere.

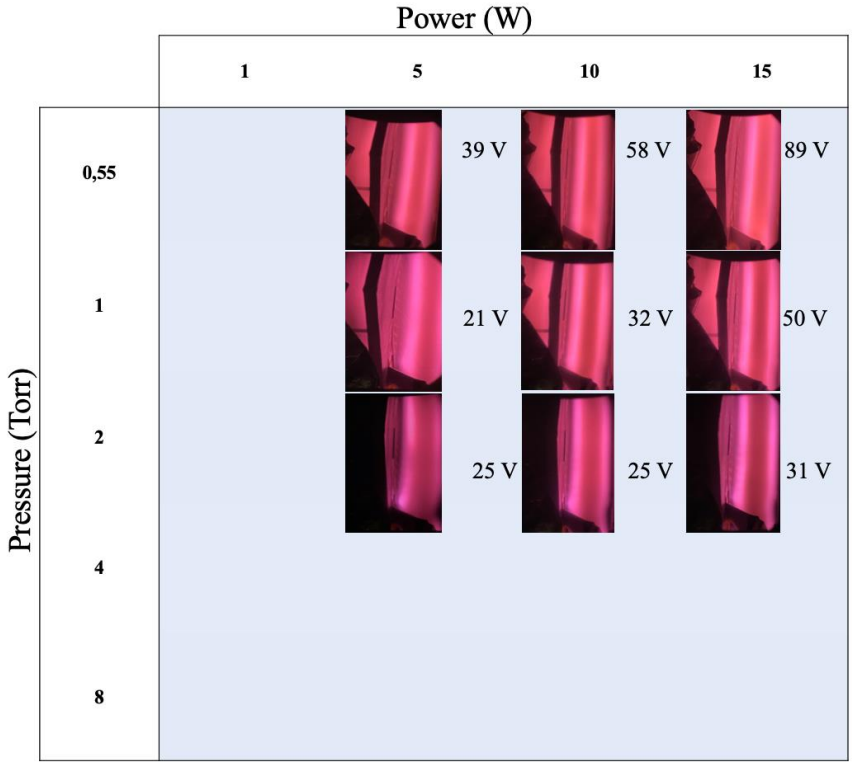

Table B 5 - Matrix of Power vs Pressure for the generator GAu using air as an atmosphere.

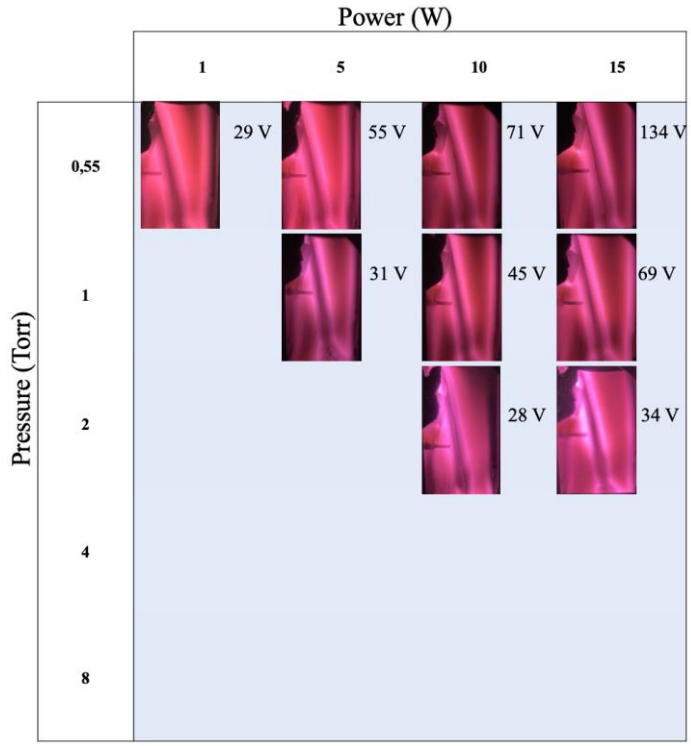

Table B 6 - Matrix of Power vs Pressure for the generator GTi using air as an atmosphere.

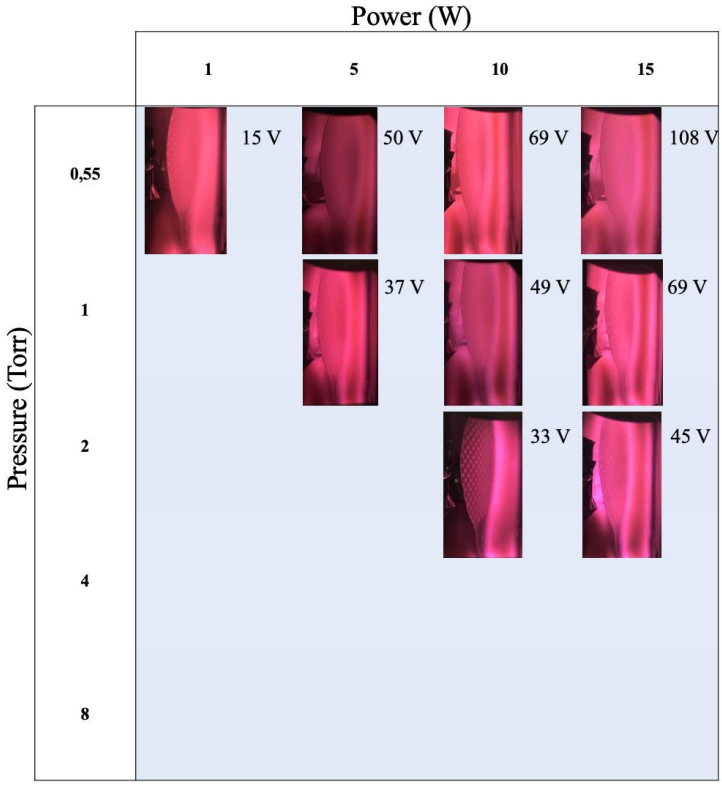

Table B 7 - Comparison of the dc self-bias potentials at a power of 10 W for the three types of gases.

	dc self-bias potential		
Pressure (Torr)	**Argon**	**Nitrogen**	**Air**
0,55	80 V	67 V	58 V
1	57 V	41 V	36 V
2	35 V	30 V	24 V
4	20 V	-	30 V

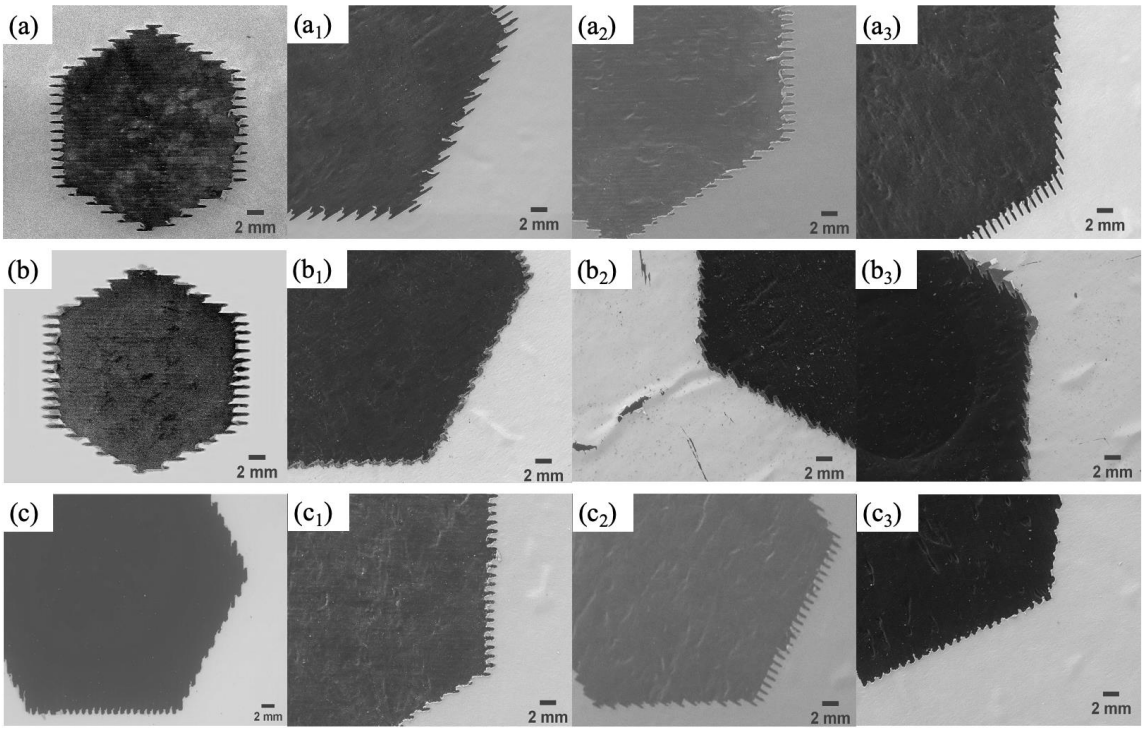

Figure B 9 - SEM images before plasma generation for generator (a) GAl, (b) GAu, and (c) GTi. Generation of plasma under (a_1) argon, (a_2) nitrogen, and (a_3) air atmospheres for generator GAl. Generation of plasma under (b_1) argon, (b_2) nitrogen, and (b_3) air atmospheres for generator GAu. Generation of plasma under (c_1) argon, (c_2) nitrogen, and (c_3) air atmospheres for generator GTi.

Figure B 10 - Generator GAu after generating plasma using argon as the discharge gas.

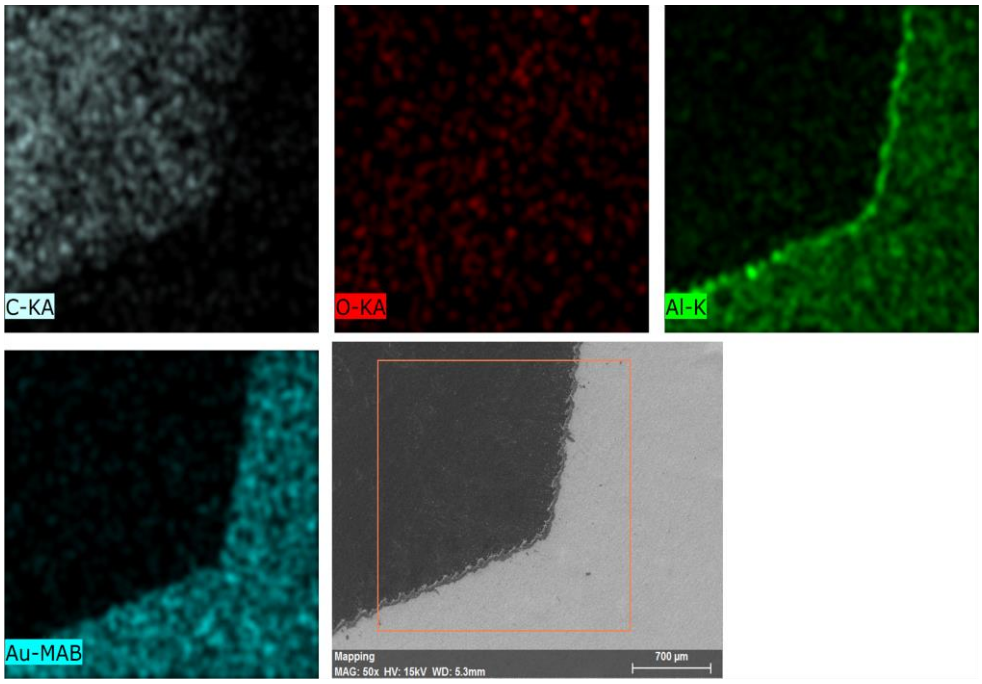

Figure B 11 - EDS elemental mapping of the generator GAu after generating plasma using argon as the discharge gas.

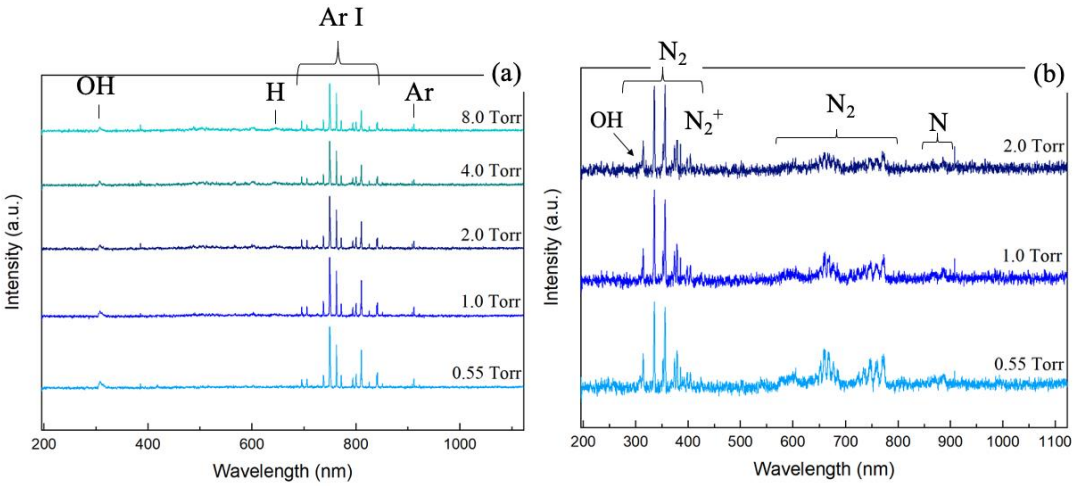

Figure B 12 - Influence of pressure on the intensity of the spectral lines for generator GAl under (a) argon atmosphere; and (b) nitrogen atmosphere, applying 10 W.

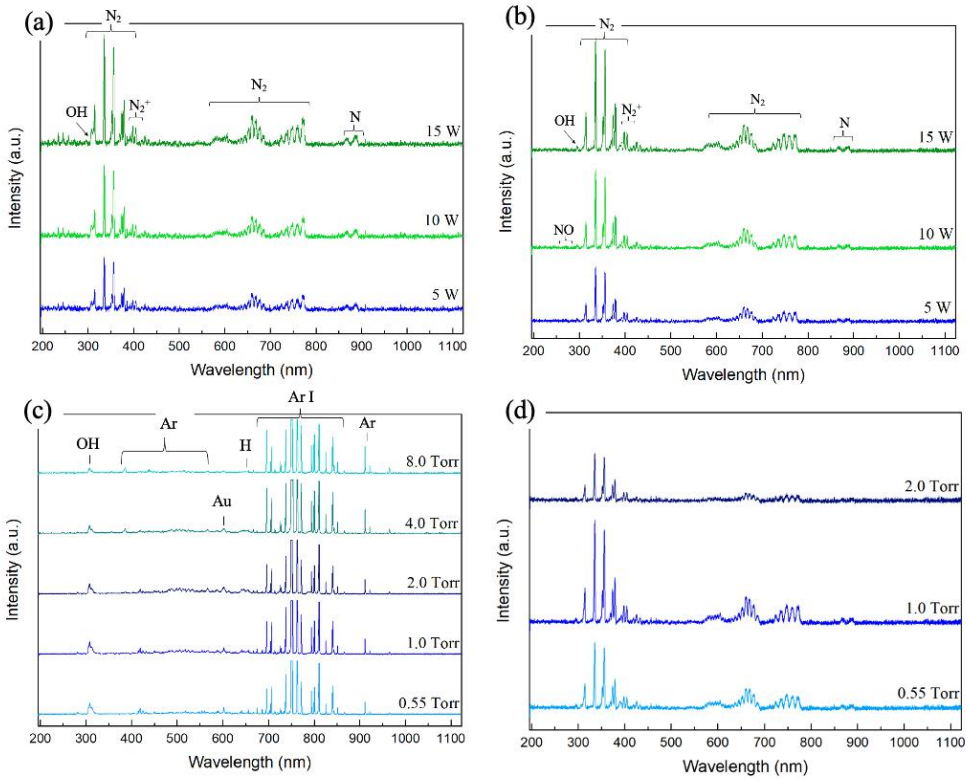

Figure B 13 – Optical emission spectra of generator GAu for (a) nitrogen atmosphere, and (b) air atmosphere, under a pressure of 1 Torr. Influence of pressure on the intensity of the spectral lines for generator GAu under (c) argon atmosphere, and (d) air atmosphere, applying 10 W.

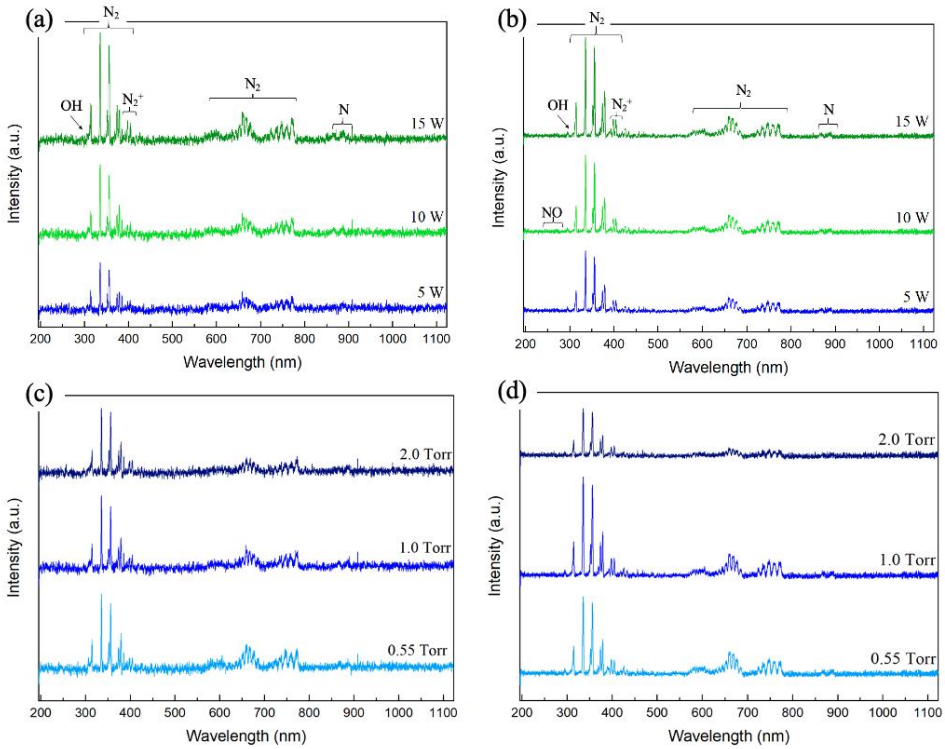

Figure B 14 - Optical emission spectra of generator GTi for (a) nitrogen atmosphere, and (b) air atmosphere, under a pressure of 1 Torr. Influence of pressure on the intensity of the spectral lines for generator GTi under (c) nitrogen atmosphere, and (d) air atmosphere, applying 10 W.

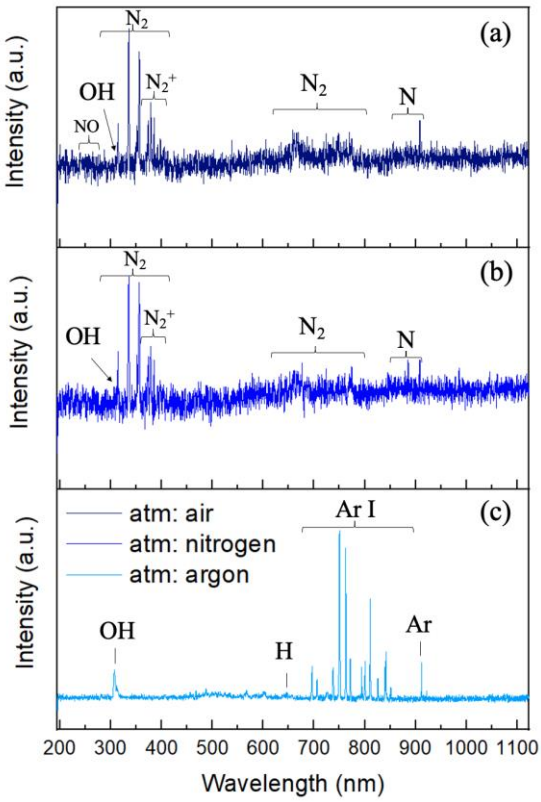

Figure B 15 - Optical emission spectra obtained of the miniaturized generators GAl: (a) air atmosphere; (b) nitrogen atmosphere; (c) argon atmosphere.

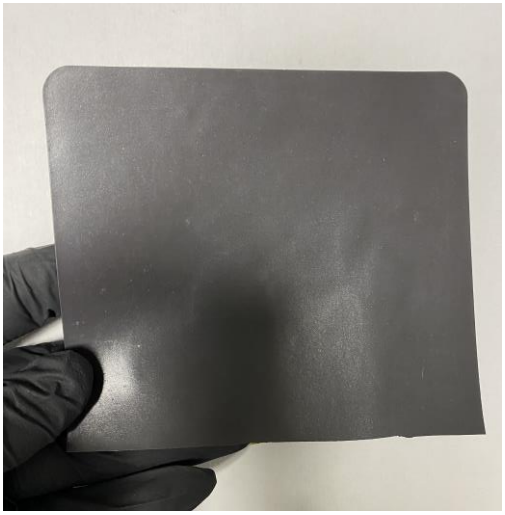

Figure B 16 - Commercial magnet used in the plasma confinement tests.

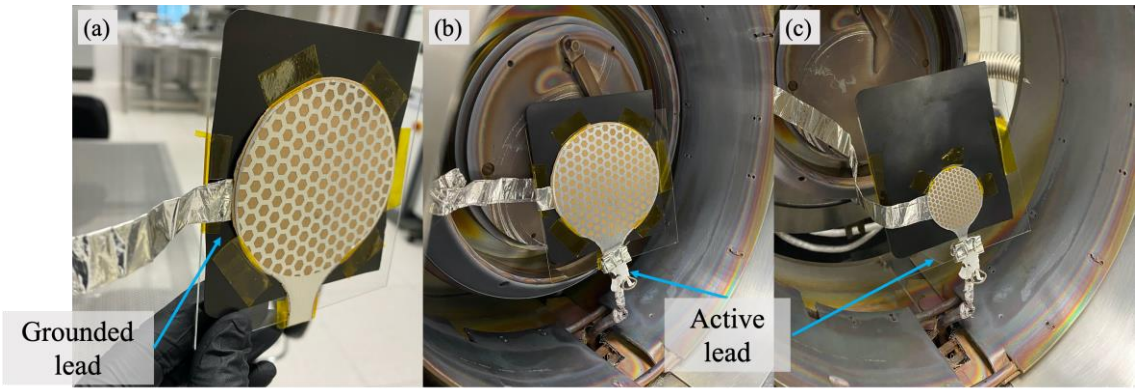

Figure B 17 - Plasma confinement tests: (a) configuration used; (b) arrangement of the generator inside the chamber; (c) arrangement of the miniaturized generator inside the chamber.